Error Estimates for Finite-Element Navier-Stokes Solvers without Standard Inf-Sup Conditions****

Jian-Guo LIU*   Jie LIU**   Robert L. PEGO***

(*Dedicated to Professor Andrew Majda on the Occasion of his* 60*th Birthday*)

Abstract   The authors establish error estimates for recently developed finite-element methods for incompressible viscous flow in domains with no-slip boundary conditions. The methods arise by discretization of a well-posed extended Navier-Stokes dynamics for which pressure is determined from current velocity and force fields. The methods use C^1 elements for velocity and C^0 elements for pressure. A stability estimate is proved for a related finite-element projection method close to classical time-splitting methods of Orszag, Israeli, DeVille and Karniadakis.

1 Introduction

Consider the Navier-Stokes equations (NSE) for incompressible fluid flow in a domain Ω in $\mathbb{R}^N$ ($N = 2$ or 3) with no-slip boundary conditions on $\Gamma := \partial\Omega$:

$$\partial_t \boldsymbol{u} + \boldsymbol{u} \cdot \nabla \boldsymbol{u} + \nabla p = \nu \Delta \boldsymbol{u} + \boldsymbol{f}, \quad \text{in } \Omega, \tag{1.1}$$

$$\nabla \cdot \boldsymbol{u} = 0, \qquad\qquad\qquad \text{in } \Omega, \tag{1.2}$$

$$\boldsymbol{u} = 0, \qquad\qquad\qquad\quad\; \text{on } \Gamma. \tag{1.3}$$

where $\boldsymbol{u}$ is the fluid velocity, p is the pressure, and $\nu = \frac{1}{\text{Re}}$ is the kinematic viscosity coefficient, assumed to be a fixed positive constant. Below, we denote the inner product of functions f and g in $L^2(\Omega)$ by $\langle f, g \rangle_\Omega$ and let $\| \cdot \|_\Omega$ denote the corresponding norm, omitting the subscript if obvious in context. The vector $\boldsymbol{n}$ denotes an outward unit normal to Γ.

The incompressibility constraint has long been a source of difficulties in both analysis and computation for NSE in bounded domains. We will study discretization schemes that relate to a well-posed extension of the dynamics of the NSE system (1.1)–(1.3), in which the incompressibility constraint (1.2) is replaced by a weak-form Poisson equation for the pressure. Up to a spatial constant, the pressure is determined by requiring

$$\langle \nabla p, \nabla q \rangle = \langle \boldsymbol{f} - \boldsymbol{u} \cdot \nabla \boldsymbol{u}, \nabla q \rangle + \nu \langle \nabla \times \boldsymbol{u}, \boldsymbol{n} \times \nabla q \rangle_\Gamma, \quad \forall\, q \in H^1(\Omega). \tag{1.4}$$

This is implied by (1.1)–(1.3) through dotting (1.1) with ∇q, using the vector identity $\Delta \boldsymbol{u} - \nabla\nabla \cdot \boldsymbol{u} = -\nabla \times \nabla \times \boldsymbol{u}$, and integrating by parts. In our previous paper [20], the system of equations consisting of (1.1), (1.3) and (1.4), but omitting (1.2), was proved to be well-posed locally in time, for strong solutions in C^3 domains with arbitrary initial data $\boldsymbol{u}_{\text{in}} \in H_0^1(\Omega, \mathbb{R}^N)$. For solutions in general, $\nabla \cdot \boldsymbol{u}$ is non-zero and satisfies a heat equation with no-flux boundary conditions. But the divergence $\nabla \cdot \boldsymbol{u}$ is zero for all time if initially so, yielding the usual solution of NSE. The well-posedness proof is based on estimates showing that the pressure gradient determined by (1.4) is strictly dominated by the viscosity term in (1.1) at leading order.

In this paper, we refer to equations (1.1), (1.3) and (1.4) as the unconstrained Navier-Stokes equations (UNSE). For analysis of equivalent and related formulations also see [10, 11]. See [25] for recent discussion of the longstanding problem of replacing the divergence constraint by a pressure Poisson equation, and an interesting alternative formulation.

The well-posedness proof in [20] was based on showing the stability of a simple time-difference scheme: Given an approximation $\boldsymbol{u}^n \in H^2 \cap H_0^1(\Omega, \mathbb{R}^N)$ to the velocity at time $t_n = n\Delta t$, we determine $\nabla p^n \in L^2(\Omega, \mathbb{R}^N)$ by requiring

$$\langle \nabla p^n, \nabla q \rangle = \langle \boldsymbol{f}^n - \boldsymbol{u}^n \cdot \nabla \boldsymbol{u}^n, \nabla q \rangle + \nu \langle \nabla \times \boldsymbol{u}^n, \boldsymbol{n} \times \nabla q \rangle, \quad \forall\, q \in H^1(\Omega), \tag{1.5}$$

then determine $\boldsymbol{u}^{n+1} \in H^2 \cap H_0^1(\Omega, \mathbb{R}^N)$ to solve

$$\frac{\boldsymbol{u}^{n+1} - \boldsymbol{u}^n}{\Delta t} - \nu \Delta \boldsymbol{u}^{n+1} = \boldsymbol{f}^n - \boldsymbol{u}^n \cdot \nabla \boldsymbol{u}^n - \nabla p^n, \quad \text{in } \Omega, \tag{1.6}$$

$$\boldsymbol{u}^{n+1} = 0, \qquad\qquad\qquad\qquad\qquad\qquad\qquad \text{on } \Gamma. \tag{1.7}$$

Intriguingly, the analysis extended easily in [20] to prove the stability of a class of fully discrete finite-element methods, in which the approximation spaces for pressure and velocity need not satisfy the classical inf-sup (LBB) criterion for stability of weak solutions in mixed methods. It is an important question to understand whether finite-element schemes can perform well without satisfying the inf-sup condition, since this condition has been a serious complication inhibiting the development and use of finite-element methods for problems involving incompressible viscous flow. As is well-known, for example, the piecewise polynomial spaces of equal order for velocity and pressure fail to be inf-sup stable. Finite element schemes based on fast Stokes solvers work well at low Reynolds number if the inf-sup condition holds, but these solvers typically converge slowly when the Reynolds number becomes high. Ways of circumventing the inf-sup condition have been developed (e.g., stabilized finite-element methods), but at the cost of additional complexity (see [2]) or for just the lowest-order velocity-pressure pairs (see [3]).

Our aim in the present paper is to investigate further the performance of the class of finite-element methods treated in [20], which derived from the work of Johnston and Liu [16]. We will establish error estimates for these schemes (higher-order in space and first-order in time), and examine their performance numerically for a smooth test problem and for benchmark tests involving flow in a driven cavity and over a backward-facing step.

We will also compare the performance of some closely related methods that incorporate an approximate Leray projection on divergence-free velocity fields. These projection methods suppress divergence errors in a more robust way that appears to be useful in numerical tests such as flow over a backward-facing step, for which the flow field may fail to have sufficient spatial regularity. The projection schemes we treat are essentially finite-element versions of classic projection methods described in work of Orszag, Israeli, DeVille and Karniadakis [17, 24] and studied recently by Leriche et al [22]. These schemes involve improved pressure boundary conditions that figured in many later developments of projection methods (see e.g. [4, 12, 15, 17, 27]). For a comprehensive recent review of projection schemes, see [12]. Also see [20] for discussion of the relation of the Johnston-Liu scheme and its C^1 analog to schemes of Kim and Moin [18], Timmermans et al [27], Henshaw and Petersson [15], Brown et al [4], and the gauge method of E and Liu [7].

A difference between the schemes we study and classic projection methods is that we determine pressure directly by discretization of the well-posed formula (1.4). In this paper, we will also prove a nonlinear stability result for the simplest finite-element projection method of this type, one that is formally first-order in time and is a variant of the schemes studied in [20]. Again, for this stability result to hold, the finite-element spaces for velocity and pressure need not be related in any way; there is no need for the classic inf-sup condition.

What our analysis does require at present is that finite elements for pressure be C^0 and finite elements for velocity be C^1. Computationally, it is generally not so attractive to use C^1 finite elements, due to the complexity and expense of solving biharmonic-type equations. However, the analysis that we perform for these fully discrete schemes provides fundamental support for a design philosophy that more practical C^0 schemes may be based upon.

Our numerical analysis relies heavily on an estimate of the part of the pressure due to viscosity, called the Stokes pressure $p_{\mathrm{s}} = p_{\mathrm{s}}(\boldsymbol{u})$ in [20] and determined from any $\boldsymbol{u} \in H^2(\Omega, \mathbb{R}^N)$ by the requirement

$$\langle \nabla p_{\mathrm{s}}, \nabla q \rangle = \langle \nabla \times \boldsymbol{u}, \boldsymbol{n} \times \nabla q \rangle_\Gamma, \quad \forall q \in H^1(\Omega). \tag{1.8}$$

The Stokes pressure is a harmonic function, solving the boundary value problem

$$\Delta p_{\mathrm{s}} = 0 \quad \text{in } \Omega, \quad \boldsymbol{n} \cdot \nabla p_{\mathrm{s}} = -\boldsymbol{n} \cdot \nabla \times \nabla \times \boldsymbol{u} \quad \text{on } \Gamma. \tag{1.9}$$

Since the right-hand side of (1.8) equals $\langle \Delta \boldsymbol{u} - \nabla \nabla \cdot \boldsymbol{u}, \nabla q \rangle$, it follows

$$\nabla p_{\mathrm{s}}(\boldsymbol{u}) = (I - \mathcal{P})(\Delta \boldsymbol{u} - \nabla \nabla \cdot \boldsymbol{u}) = (\Delta \mathcal{P} - \mathcal{P}\Delta)\boldsymbol{u}. \tag{1.10}$$

Here $\mathcal{P}$ denotes the Leray-Helmholtz projection operator onto divergence-free fields with zero normal component, providing the Helmholtz decomposition $\boldsymbol{u} = \mathcal{P}\boldsymbol{u} + \nabla\phi$, where

$$\langle \mathcal{P}\boldsymbol{u}, \nabla q \rangle = \langle \boldsymbol{u} - \nabla\phi, \nabla q \rangle = 0, \quad \forall q \in H^1(\Omega). \tag{1.11}$$

A central tool is the following result proved in [20], showing that the commutator (1.10) between the Laplacian and Leray projection operators is strictly dominated by the viscosity term at leading order.

Theorem 1.1 *Let $\Omega \subset \mathbb{R}^N$ ($N \geq 2$) be a connected bounded domain with C^3 boundary. Then for any $\varepsilon > 0$, there exists $C \geq 0$ such that for all vector fields $\boldsymbol{u} \in H^2 \cap H_0^1(\Omega, \mathbb{R}^N)$,*

$$\int_\Omega |(\Delta \mathcal{P} - \mathcal{P}\Delta)\boldsymbol{u}|^2 \leq \left(\frac{1}{2} + \varepsilon\right) \int_\Omega |\Delta \boldsymbol{u}|^2 + C \int_\Omega |\nabla \boldsymbol{u}|^2. \tag{1.12}$$

The rest of this paper is organized as follows. In the next section, we establish error estimates for the basic class of finite-element schemes treated in [20]. In Section 3, we prove a stability theorem for a related projection method. The numerical analysis is based on Theorem 1.1 and is limited to C^3 domains — it is an open question whether similar results hold in domains with corners, particularly in domains where H^2 regularity may fail naturally due to corner singularities.

We discuss several practical issues in Section 4, related to non-homogeneous boundary conditions for velocity, numerical treatment of re-entrant corners, higher-order time discretization, and how to compute the pressure. Then in Section 5, we present and discuss numerical results for the finite-element schemes that we study. We conclude in Section 6 with a discussion of the relation of our results to the inf-sup condition in the time-independent linear case.

2 Error Estimates for Extended Navier-Stokes Dynamics

Since pressure is determined directly from current velocity and forcing fields in the UNSE system, discretization is rather straightforward, as indicated already by Johnston and Liu [16]. An implicit treatment of the viscosity term is appropriate for low to moderate Reynolds number flow, but for efficiency and simplicity, we discretize the remaining terms explicitly in time. For the spatial discretization, let $Y_h \subset H^1(\Omega)/\mathbb{R}$ be a space of C^0 finite elements for pressure, and $X_{0,h} \subset H^2 \cap H_0^1(\Omega, \mathbb{R}^N)$ be a space of C^1 finite elements for velocity. Here $h > 0$ is a bounded discretization parameter.

The class of schemes we study is defined as follows. Given $\boldsymbol{u}_h^n \in X_{0,h}$ as an approximation to velocity at time $t_n = n\Delta t$, we determine $p_h^n \in Y_h$ through discretization of the pressure Poisson equation (1.4), by requiring

$$\langle \nabla p_h^n, \nabla q_h \rangle = \langle \boldsymbol{f}^n - \boldsymbol{u}_h^n \cdot \nabla \boldsymbol{u}_h^n, \nabla q_h \rangle + \nu \langle \nabla \times \boldsymbol{u}_h^n, \boldsymbol{n} \times \nabla q_h \rangle_\Gamma, \quad \forall q_h \in Y_h. \tag{2.1}$$

Then we find $\boldsymbol{u}_h^{n+1} \in X_{0,h}$ so that

$$\left\langle \frac{\nabla \boldsymbol{u}_h^{n+1} - \nabla \boldsymbol{u}_h^n}{\Delta t}, \nabla \boldsymbol{v}_h \right\rangle + \nu \langle \Delta \boldsymbol{u}_h^{n+1}, \Delta \boldsymbol{v}_h \rangle = \langle \nabla p_h^n - \boldsymbol{f}^n + \boldsymbol{u}_h^n \cdot \nabla \boldsymbol{u}_h^n, \Delta \boldsymbol{v}_h \rangle \tag{2.2}$$

for all $\boldsymbol{v}_h \in X_{0,h}$. This scheme is analogous to a C^0 scheme described by Johnston and Liu [16], the difference being that to derive the weak form of (1.1), instead of dotting with $\boldsymbol{v}_h$, we dot with $\Delta \boldsymbol{v}_h$ to get (2.2).

In this section, we prove the following error estimates for (2.1)–(2.2), which ensure high-order accuracy in space given a sufficiently smooth solution of the UNSE system for $t \geq 0$.

Similar to the stability proof in [20], the proof is based on H^1 estimates and crucially uses the estimate on Stokes pressure from Theorem 1.1. Thus the result is limited to C^3 domains and to initial data that satisfy nonlocal compatibility conditions implied by UNSE. We are not aware, however, of any previous results of this type for fully nonlinear NSE that treat viscosity terms implicitly, and nonlinear and pressure terms explicitly in general domains with smooth boundary.

Theorem 2.1 *Assume Ω is a bounded domain in $\mathbb{R}^N$ $(N = 2, 3)$ with C^3 boundary. Let $M_0, \nu > 0$, and let $T_* > 0$ be given by the Stability Theorem 4.1 in [20]. Let $m \geq 2$, $m' \geq 2$ be integers, and assume that*

(i) *The spaces $X_{0,h} \subset H^2 \cap H_0^1(\Omega, \mathbb{R}^N)$ and $Y_h \subset H^1(\Omega)$ have the property that whenever $0 < h < 1$, $\boldsymbol{v} \in H^{m+1} \cap H_0^1(\Omega, \mathbb{R}^N)$ and $q \in H^{m'}(\Omega)$,*

$$\inf_{\boldsymbol{v}_h \in X_{0,h}} \|\Delta(\boldsymbol{v} - \boldsymbol{v}_h)\| \leq C_0 h^{k-1} \|\boldsymbol{v}\|_{H^{k+1}} \quad \text{for } k = 2 \text{ and } m, \tag{2.3}$$

$$\inf_{q_h \in Y_h} \|\nabla(q - q_h)\| \leq C_0 h^{m'-1} \|q\|_{H^{m'}}, \tag{2.4}$$

where $C_0 > 0$ is independent of $\boldsymbol{v}$, q and h.

(ii) *$\boldsymbol{f} \in C^1([0, T], L^2(\Omega, \mathbb{R}^N))$, $T > 0$, and a given solution of (1.1), (1.3) and (1.4) satisfies*

$$(\boldsymbol{u}, p) \in C^1([0, T]; H^{m+1}(\Omega, \mathbb{R}^N)) \times C^1([0, T]; H^{m'}(\Omega)/\mathbb{R}).$$

Then there exists $C_1 > 0$ with the following property. Whenever $\boldsymbol{u}_h^0 \in X_{0,h}$, $0 < h < 1$, $0 < n\Delta t \leq \min(T, T_*)$, and

$$\|\nabla \boldsymbol{u}_h^0\|^2 + \nu \Delta t \|\Delta \boldsymbol{u}_h^0\|^2 + \sum_{k=0}^{n} \|\boldsymbol{f}(t_k)\|^2 \Delta t \leq M_0, \tag{2.5}$$

the velocity and pressure errors $\boldsymbol{e}^n = \boldsymbol{u}(t_n) - \boldsymbol{u}_h^n$, $r^n = p(t_n) - p_h^n$ for the solution to the finite-element scheme (2.1) and (2.2) satisfy

$$\sup_{0 \leq k \leq n} \|\nabla \boldsymbol{e}^k\|^2 + \sum_{k=0}^{n} (\|\Delta \boldsymbol{e}^k\|^2 + \|\nabla r^k\|^2)\Delta t$$
$$\leq C_1(\Delta t^2 + h^{2m-2} + h^{2m'-2} + \|\nabla \boldsymbol{e}^0\|^2 + \|\Delta \boldsymbol{e}^0\|^2 \Delta t). \tag{2.6}$$

Remark 2.1 When $m = m'$, the time-averaged error estimates for velocity in H^2 and pressure in H^1 have optimal convergence rates in terms of the approximation assumptions (2.3) and (2.4). For typical C^1 finite element spaces $X_{0,h}$, whose element restrictions contain all polynomials of degree d, standard results for polygonal domains with quasi-uniform meshes assert that (2.3) holds when $2 \leq m \leq d$. Similarly, for C^0 finite element spaces Y_h, whose element restrictions include all polynomials of degree d', (2.4) holds for $2 \leq m' \leq d' + 1$. Theorem 2.1 does not apply in domains with corners, but for smooth enough solutions, the convergence rate from (2.6) would be optimal (the same as interpolation error) for both velocity and pressure provided that $d' + 1 = d$. (The theorem can be applied in principle in the case of C^3 domains, if suitable parametrically mapped piecewise polynomial finite elements are used.) For the FVS (locally cubic) C^1 finite elements used in our numerical tests, hypothesis (2.3)

holds for both $m = 2$ and 3, and hypothesis (2.4) holds for both $m' = 3$ and 4 (see [6, §6.1.5, p. 357]); for smooth solutions, the best rate in (2.6) would then correspond to $m = m' = 3$, which is not optimal for pressure. In our tests, though, we actually observe optimal convergence rates for both velocity and pressure (see Section 5 below).

Proof Let $M_0, \nu > 0$ and let T_*, C_* be given by [20, Theorem 4.1]. Fix integers $m \geq 2$ and $m' \geq 1$. Let $C_0 > 0$ and suppose that $X_{0,h}, Y_h$ satisfy assumption (i) of Theorem 2.1. Suppose that T, $\boldsymbol{f}$, $\boldsymbol{u}$ and p satisfy assumption (ii), so that (1.1) and (1.2) hold. The pressure p then satisfies (1.4). More generally, we can suppose that $\boldsymbol{u}$ and p satisfy the unconstrained system UNSE consisting of (1.1), (1.3) and (1.4), without (1.2).

In what follows, C denotes a generic constant independent of Δt and h, whose value may change from case to case. (The value of C will depend on the solution, so it may depend on quantities such as ν in ways that we will not attempt to track here.)

2.1 Approximation error

We first project the solution into the finite element spaces and estimate the resulting approximation error. Define projections $\boldsymbol{\Pi}_h$ on $H^2 \cap H_0^1(\Omega, \mathbb{R}^N)$ and $\mathbf{P}_h$ on $H^1(\Omega)/\mathbb{R}$ as follows. Given any $\boldsymbol{a} \in H^2 \cap H_0^1(\Omega, \mathbb{R}^N)$ and $b \in H^1(\Omega)/\mathbb{R}$, we define

$$\boldsymbol{a}_h = \boldsymbol{\Pi}_h \boldsymbol{a} \in X_{0,h}, \quad b_h = \mathbf{P}_h b \in Y_h \tag{2.7}$$

as the solutions of the following weak-form Poisson equations:

$$\langle \Delta \boldsymbol{a}_h, \Delta \boldsymbol{v}_h \rangle = \langle \Delta \boldsymbol{a}, \Delta \boldsymbol{v}_h \rangle, \quad \forall \boldsymbol{v}_h \in X_{0,h}, \tag{2.8}$$

$$\langle \nabla b_h, \nabla q_h \rangle = \langle \nabla b, \nabla q_h \rangle, \quad \forall q_h \in Y_h. \tag{2.9}$$

Notice that since $\langle \Delta(\boldsymbol{a} - \boldsymbol{a}_h), \Delta \boldsymbol{a}_h \rangle = 0$,

$$\|\Delta \boldsymbol{a}\|^2 = \|\Delta \boldsymbol{a}_h\|^2 + \|\Delta(\boldsymbol{a} - \boldsymbol{a}_h)\|^2. \tag{2.10}$$

Moreover, we have the following basic estimates.

Lemma 2.1 *For any* $\boldsymbol{a} \in H^2 \cap H_0^1(\Omega, \mathbb{R}^N)$, $b \in H^1(\Omega)/\mathbb{R}$,

$$\|\Delta(\boldsymbol{a} - \boldsymbol{a}_h)\| \leq \inf_{\boldsymbol{v}_h \in X_{0,h}} \|\Delta(\boldsymbol{a} - \boldsymbol{v}_h)\|, \tag{2.11}$$

$$\|\nabla(b - b_h)\| \leq \inf_{q_h \in Y_h} \|\nabla(b - q_h)\|, \tag{2.12}$$

$$\|\nabla(\boldsymbol{a} - \boldsymbol{a}_h)\| \leq Ch\|\Delta(\boldsymbol{a} - \boldsymbol{a}_h)\|. \tag{2.13}$$

Proof For any $\boldsymbol{v}_h \in X_{0,h}$,

$$\langle \Delta(\boldsymbol{a} - \boldsymbol{a}_h), \Delta(\boldsymbol{a} - \boldsymbol{a}_h) \rangle = \langle \Delta(\boldsymbol{a} - \boldsymbol{a}_h), \Delta(\boldsymbol{a} - \boldsymbol{v}_h) \rangle + \langle \Delta(\boldsymbol{a} - \boldsymbol{a}_h), \Delta(\boldsymbol{v}_h - \boldsymbol{a}_h) \rangle.$$

The last term is zero because of (2.8), hence the Cauchy-Schwartz inequality gives (2.11). Similarly, one can prove (2.12). To prove (2.13), define $\boldsymbol{w} \in H^3 \cap H_0^1$ to be the solution of

$$-\Delta \boldsymbol{w} = \boldsymbol{a} - \boldsymbol{a}_h. \tag{2.14}$$

By assumption (2.3) with $k = 2$, there exists $\boldsymbol{w}_h \in X_{0,h}$ such that

$$\|\Delta(\boldsymbol{w} - \boldsymbol{w}_h)\| \leq Ch\|\boldsymbol{w}\|_{H^3} \leq Ch\|\nabla(\boldsymbol{a} - \boldsymbol{a}_h)\|,$$

where we have used elliptic regularity for (2.14). So

$$\begin{aligned}
\|\nabla(\boldsymbol{a} - \boldsymbol{a}_h)\|^2 &= \langle -\Delta(\boldsymbol{a} - \boldsymbol{a}_h), \boldsymbol{a} - \boldsymbol{a}_h \rangle = \langle \Delta(\boldsymbol{a} - \boldsymbol{a}_h), \Delta\boldsymbol{w} \rangle \\
&= \langle \Delta(\boldsymbol{a} - \boldsymbol{a}_h), \Delta(\boldsymbol{w} - \boldsymbol{w}_h) \rangle \\
&\leq \|\Delta(\boldsymbol{a} - \boldsymbol{a}_h)\| \cdot Ch\|\nabla(\boldsymbol{a} - \boldsymbol{a}_h)\|.
\end{aligned}$$

This proves (2.13).

Given our regularity and approximation assumptions (i) and (ii), we can conclude that with the notation

$$\boldsymbol{u}_h(t_n) = \boldsymbol{\Pi}_h \boldsymbol{u}(t_n), \quad p_h(t_n) = \mathbf{P}_h p(t_n), \tag{2.15}$$

the error of approximating the solution by its projection is estimated by

$$\|\Delta(\boldsymbol{u}(t_n) - \boldsymbol{u}_h(t_n))\| \leq Ch^{m-1}, \quad \|\nabla(p(t_n) - p_h(t_n))\| \leq Ch^{m'-1}. \tag{2.16}$$

2.2 Discretization error for pressure

It remains to estimate the discretization or scheme errors

$$\boldsymbol{e}_h^n = \boldsymbol{u}_h(t_n) - \boldsymbol{u}_h^n, \quad r_h^n = p_h(t_n) - p_h^n. \tag{2.17}$$

We first focus on estimating the pressure error r_h^n in this subsection. Our aim is to show that for any $\varepsilon_0 > 0$, there exists $C > 0$, such that whenever $0 < n\Delta t \leq \min(T, T_*)$, we have

$$\|\nabla r_h^n\|^2 \leq \left(\frac{1}{2} + \varepsilon_0\right)\nu^2\|\Delta\boldsymbol{e}_h^n\|^2 + C\|\nabla\boldsymbol{e}_h^n\|^2 + Ch^{2m-2}. \tag{2.18}$$

Recall that for any $q_h \in H^1(\Omega)$, the exact pressure satisfies

$$\begin{aligned}
\langle \nabla p(t_n), \nabla q_h \rangle &= \langle \boldsymbol{f}(t_n) - \boldsymbol{u}(t_n) \cdot \nabla\boldsymbol{u}(t_n), \nabla q_h \rangle - \nu\langle \nabla \times \nabla \times \boldsymbol{u}(t_n), \nabla q_h \rangle \\
&= \langle \boldsymbol{f}(t_n) - \boldsymbol{u}_h(t_n) \cdot \nabla\boldsymbol{u}_h(t_n), \nabla q_h \rangle - \nu\langle \nabla \times \nabla \times \boldsymbol{u}_h(t_n), \nabla q_h \rangle - \ell_n, \quad \tag{2.19}
\end{aligned}$$

where

$$\begin{aligned}
\ell_n &= \langle (I - \boldsymbol{\Pi}_h)\boldsymbol{u}(t_n) \cdot \nabla\boldsymbol{u}(t_n) + \boldsymbol{u}_h(t_n) \cdot \nabla(I - \boldsymbol{\Pi}_h)\boldsymbol{u}(t_n), \nabla q_h \rangle \\
&\quad + \nu\langle \nabla \times \nabla \times (I - \boldsymbol{\Pi}_h)\boldsymbol{u}(t_n), \nabla q_h \rangle.
\end{aligned}$$

By Lemma 2.1, one has

$$|\ell_n| \leq C(h^m + \nu h^{m-1})\|\nabla q_h\| \leq Ch^{m-1}\|\nabla q_h\|. \tag{2.20}$$

Subtracting (2.1) from (2.19), we get

$$\langle \nabla r_h^n, \nabla q_h \rangle = -\langle \boldsymbol{e}_h^n \cdot \nabla\boldsymbol{u}_h(t_n) + \boldsymbol{u}_h^n \cdot \nabla\boldsymbol{e}_h^n, \nabla q_h \rangle - \nu\langle (I - \mathcal{P})\nabla \times \nabla \times \boldsymbol{e}_h^n, \nabla q_h \rangle - \ell_n, \quad \tag{2.21}$$

where we have used $\langle \mathcal{P}\nabla \times \nabla \times \boldsymbol{e}_h^n, \nabla q_h \rangle = 0$. Take $q_h = r_h^n$ and let

$$\mathrm{I}_1 = \nu\|(I-\mathcal{P})\nabla \times \nabla \times \boldsymbol{e}_h^n\|, \quad \mathrm{I}_2 = \|\boldsymbol{e}_h^n \cdot \nabla \boldsymbol{u}_h(t_n)\|, \quad \mathrm{I}_3 = \|\boldsymbol{u}_h^n \cdot \nabla \boldsymbol{e}_h^n\|.$$

By the Cauchy-Schwartz inequality, we get that for any $\varepsilon_1 > 0$,

$$\|r_h^n\|^2 \leq (\mathrm{I}_1 + \mathrm{I}_2 + \mathrm{I}_3 + Ch^{m-1})^2 \leq \mathrm{I}_1^2(1+\varepsilon_1) + \frac{1}{\varepsilon_1}(\mathrm{I}_2 + \mathrm{I}_3 + Ch^{m-1})^2. \tag{2.22}$$

We estimate the terms as follows. By identity (3.2) and (1.10), we have

$$-(I-\mathcal{P})\nabla \times \nabla \times \boldsymbol{e}_h^n = (\Delta\mathcal{P} - \mathcal{P}\Delta)\boldsymbol{e}_h^n.$$

Therefore by Theorem 1.1, we get the estimate

$$\|(I-\mathcal{P})\nabla \times \nabla \times \boldsymbol{e}_h^n\|^2 \leq \left(\frac{1}{2} + \varepsilon_1\right)\|\Delta\boldsymbol{e}_h^n\|^2 + C\|\nabla\boldsymbol{e}_h^n\|^2. \tag{2.23}$$

Next recall that, as in [20], by the Sobolev embedding theorems and Ladyzhenskaya's inequalities, we have

$$\int_\Omega |\boldsymbol{u}\cdot\nabla\boldsymbol{v}|^2 \leq \left(\int_\Omega |\boldsymbol{u}|^6\right)^{\frac{1}{3}}\left(\int_\Omega |\nabla\boldsymbol{v}|^3\right)^{\frac{2}{3}} \leq C\|\nabla\boldsymbol{u}\|^2\|\nabla\boldsymbol{v}\|\|\nabla\boldsymbol{v}\|_{H^1}. \tag{2.24}$$

We can use the regularity assumption (ii) together with the approximation bounds (2.16) to bound terms involving $\boldsymbol{u}_h(t_n)$, and the stability result in Theorem 3.1 to conclude that as long as (2.5) holds and $0 < n\Delta t \leq \min(T, T_*)$, we have $\|\nabla\boldsymbol{u}_h^n\| \leq C$ and hence

$$\|\boldsymbol{e}_h^n \cdot \nabla\boldsymbol{u}_h(t_n)\|^2 \leq C\|\nabla\boldsymbol{e}_h^n\|^2\|\nabla\boldsymbol{u}_h(t_n)\|\|\nabla\boldsymbol{u}_h(t_n)\|_{H^1} \leq C\|\nabla\boldsymbol{e}_h^n\|^2, \tag{2.25}$$

$$\|\boldsymbol{u}_h^n \cdot \nabla\boldsymbol{e}_h^n\|^2 \leq C\|\nabla\boldsymbol{u}_h^n\|^2\|\nabla\boldsymbol{e}_h^n\|\|\nabla\boldsymbol{e}_h^n\|_{H^1} \leq C\|\nabla\boldsymbol{e}_h^n\|\|\Delta\boldsymbol{e}_h^n\|. \tag{2.26}$$

In particular, we obtain

$$\frac{2}{\varepsilon_1}\mathrm{I}_3^2 \leq \frac{2C}{\varepsilon_1}\|\nabla\boldsymbol{e}_h^n\|\|\Delta\boldsymbol{e}_h^n\| \leq \varepsilon_1\nu^2\|\Delta\boldsymbol{e}_h^n\|^2 + \frac{C^2}{\varepsilon_1^3\nu^2}\|\nabla\boldsymbol{e}_h^n\|^2. \tag{2.27}$$

Combining this with (2.25) and (2.23), from (2.22), we see that if ε_1 is chosen sufficiently small we get (2.18).

2.3 Discretization error for velocity

If we integrate (1.1) from t_n to t_{n+1} and use the regularity assumption (ii), we see that the exact solution satisfies, for any $\boldsymbol{v}_h \in X_{0,h}$,

$$\left\langle \frac{1}{\Delta t}(\nabla\boldsymbol{u}(t_{n+1}) - \nabla\boldsymbol{u}(t_n)), \nabla\boldsymbol{v}_h \right\rangle + \nu\langle \Delta\boldsymbol{u}(t_{n+1}), \Delta\boldsymbol{v}_h \rangle$$
$$= \langle \nabla p(t_n) + \boldsymbol{u}(t_n)\cdot\nabla\boldsymbol{u}(t_n) - \boldsymbol{f}(t_n) + \boldsymbol{g}^n\Delta t, \Delta\boldsymbol{v}_h \rangle, \tag{2.28}$$

where $\|\boldsymbol{g}^n\|$ is uniformly bounded in n. Using the projections in (2.15), we can rewrite this as

$$\left\langle \frac{1}{\Delta t}(\nabla\boldsymbol{u}_h(t_{n+1}) - \nabla\boldsymbol{u}_h(t_n)), \nabla\boldsymbol{v}_h \right\rangle + \nu\langle \Delta\boldsymbol{u}_h(t_{n+1}), \Delta\boldsymbol{v}_h \rangle$$
$$= \langle \nabla p_h(t_n) + \boldsymbol{u}_h(t_n)\cdot\nabla\boldsymbol{u}_h(t_n) - \boldsymbol{f}(t_n) + \boldsymbol{g}^n\Delta t, \Delta\boldsymbol{v}_h \rangle + \widehat{\ell^n}, \tag{2.29}$$

where, due to (2.8),

$$\widehat{\ell^n} = -\frac{1}{\Delta t}\langle \nabla(I - \mathbf{\Pi}_h)(\boldsymbol{u}(t_{n+1}) - \boldsymbol{u}(t_n)), \nabla \boldsymbol{v}_h\rangle + \langle \nabla(I - \mathbf{P}_h)p(t_n), \Delta \boldsymbol{v}_h\rangle$$
$$+ \langle((I - \mathbf{\Pi}_h)\boldsymbol{u}(t_n)) \cdot \nabla \boldsymbol{u}(t_n) + (\mathbf{\Pi}_h\boldsymbol{u}(t_n)) \cdot \nabla(I - \mathbf{\Pi}_h)\boldsymbol{u}(t_n), \Delta \boldsymbol{v}_h\rangle. \qquad (2.30)$$

By the regularity assumptions (ii), (2.16) and (2.13) and estimates like (2.25)–(2.26) (and the elliptic regularity estimate $\|\nabla \boldsymbol{v}_h\| \leq \|\boldsymbol{v}_h\|_{H^2} \leq C\|\Delta \boldsymbol{v}_h\|$), we have

$$|\widehat{\ell^n}| \leq Ch^m\|\nabla \boldsymbol{v}_h\| + C(h^{m'-1} + h^{m-\frac{1}{2}})\|\Delta \boldsymbol{v}_h\| \leq \varepsilon_2\|\Delta \boldsymbol{v}_h\|^2 + C(h^{2m'-2} + h^{2m-1}),$$
$$|\langle \boldsymbol{g}^n\Delta t, \Delta \boldsymbol{v}_h\rangle| \leq \varepsilon_2\|\Delta \boldsymbol{v}_h\|^2 + C\Delta t^2.$$

Subtracting (2.2) from (2.29), we find that the scheme errors $\boldsymbol{e}_h^n$, r_h^n satisfy

$$\left\langle \frac{\nabla \boldsymbol{e}_h^{n+1} - \nabla \boldsymbol{e}_h^n}{\Delta t}, \nabla \boldsymbol{v}_h\right\rangle + \nu\langle \Delta \boldsymbol{e}_h^{n+1}, \Delta \boldsymbol{v}_h\rangle$$
$$= \langle \nabla r_h^n, \Delta \boldsymbol{v}_h\rangle + \langle \boldsymbol{e}_h^n \cdot \nabla \boldsymbol{u}_h(t_n) + \boldsymbol{u}_h^n \cdot \nabla \boldsymbol{e}_h^n, \Delta \boldsymbol{v}_h\rangle + \langle \boldsymbol{g}^n\Delta t, \Delta \boldsymbol{v}_h\rangle + \widehat{\ell^n}. \qquad (2.31)$$

We will take $\boldsymbol{v}_h = \boldsymbol{e}_h^{n+1}$ and estimate terms on the right-hand side as follows. First, using (2.18) we get

$$|\langle \nabla r_h^n, \Delta \boldsymbol{e}_h^{n+1}\rangle| \leq \frac{\nu}{2}\|\Delta \boldsymbol{e}_h^{n+1}\|^2 + \frac{1}{2\nu}\|\nabla r_h^n\|^2$$
$$\leq \frac{\nu}{2}\|\Delta \boldsymbol{e}_h^{n+1}\|^2 + \left(\frac{\nu}{4} + \frac{\varepsilon_0\nu}{2}\right)\|\Delta \boldsymbol{e}_h^n\|^2 + C\|\nabla \boldsymbol{e}_h^n\|^2 + Ch^{2m-2}. \qquad (2.32)$$

Using (2.25) and (2.26), we get

$$|\langle \boldsymbol{e}_h^n \cdot \nabla \boldsymbol{u}_h(t_n) + \boldsymbol{u}_h^n \cdot \nabla \boldsymbol{e}_h^n, \Delta \boldsymbol{e}_h^{n+1}\rangle| \leq \varepsilon_2\|\Delta \boldsymbol{e}_h^{n+1}\|^2 + \frac{C}{\varepsilon_2}(\|\nabla \boldsymbol{e}_h^n\|^2 + \|\nabla \boldsymbol{e}_h^n\|\|\Delta \boldsymbol{e}_h^n\|)$$
$$\leq \varepsilon_2\|\Delta \boldsymbol{e}_h^{n+1}\|^2 + \varepsilon_2\|\Delta \boldsymbol{e}_h^n\|^2 + \frac{C}{\varepsilon_2^3}\|\nabla \boldsymbol{e}_h^n\|^2. \qquad (2.33)$$

Therefore, we find that

$$\frac{1}{2\Delta t}(\|\nabla \boldsymbol{e}_h^{n+1}\|^2 - \|\nabla \boldsymbol{e}_h^n\|^2) + \left(\nu - \frac{\nu}{2} - 3\varepsilon_2\right)\|\Delta \boldsymbol{e}_h^{n+1}\|^2$$
$$\leq \left(\frac{\nu}{4} + \frac{\varepsilon_0\nu}{2} + \varepsilon_2\right)\|\Delta \boldsymbol{e}_h^n\|^2 + C\|\nabla \boldsymbol{e}_h^n\|^2 + C(\Delta t^2 + h^{2m'-2} + h^{2m-2}). \qquad (2.34)$$

Now, we can choose ε_0 and ε_2 sufficiently small so that the quantities

$$\widetilde{\varepsilon}_1 = \nu - 6\varepsilon_2, \quad \widetilde{\varepsilon}_2 = \frac{\nu}{2} - \varepsilon_0\nu - 8\varepsilon_2$$

are positive. Then we can rewrite (2.34) as

$$\frac{1}{\Delta t}(\|\nabla \boldsymbol{e}_h^{n+1}\|^2 - \|\nabla \boldsymbol{e}_h^n\|^2) + \widetilde{\varepsilon}_1(\|\Delta \boldsymbol{e}_h^{n+1}\|^2 - \|\Delta \boldsymbol{e}_h^n\|^2) + \widetilde{\varepsilon}_2\|\Delta \boldsymbol{e}_h^n\|^2$$
$$\leq C\|\nabla \boldsymbol{e}_h^n\|^2 + C(\Delta t^2 + h^{2m'-2} + h^{2m-2}). \qquad (2.35)$$

By a Gronwall-type argument similar to that in the next section below but without the cubic nonlinear terms, we deduce, provided (2.5) holds and $0 \leq n\Delta t \leq \min(T, T_*)$, that

$$\sup_{0 \leq k \leq n}\|\nabla \boldsymbol{e}_h^k\|^2 + \widetilde{\varepsilon}_1\sum_{k=0}^n\|\Delta \boldsymbol{e}_h^k\|^2\Delta t$$
$$\leq C(\Delta t^2 + h^{2m-2} + h^{2m'-2} + \|\nabla \boldsymbol{e}_h^0\|^2 + \widetilde{\varepsilon}_2\|\Delta \boldsymbol{e}_h^0\|^2\Delta t). \qquad (2.36)$$

Going back to (2.18), we get

$$\sum_{k=0}^{n} \|\nabla r_h^k\|^2 \Delta t \le C(\Delta t^2 + h^{2m-2} + h^{2m'-2} + \|\nabla e_h^0\|^2 + \widetilde{\varepsilon}_2 \|\Delta e_h^0\|^2 \Delta t). \qquad (2.37)$$

Finally, using (2.16), we can replace e_h^k and r_h^k in the two inequalities above by e^k and r^k respectively. This finishes the proof of the theorem.

3 Stability of a Projection Method

3.1 Divergence suppression by Leray projection

In numerical experiments, we have found that the simple scheme (2.1)–(2.2) (and variants with higher-order time stepping) can work well when the solution is smooth. But for more challenging problems, such as flow over a backward-facing step that involves vortex shedding behind an obtuse corner, (2.1)–(2.2) need a little extra help to suppress divergence errors that may generate sources or sinks that significantly affect the flow. Heuristically, one can see that for the time-discrete, spatially continuous scheme corresponding to (2.2), the (generally nonzero) quantity $w^n = \nabla \cdot \boldsymbol{u}^n$ satisfies

$$w^{n+1} - \nu \Delta t \Delta w^{n+1} = w^n, \qquad (3.1)$$

with boundary values determined by the solution of the Helmholtz equation satisfied by $\boldsymbol{u}^{n+1}$. Errors, introduced by spatial discretization perhaps, may build up due to the nearly neutral stability of this equation.

For this reason, we find it useful to incorporate a projection step in the computation to suppress the right-hand side of (3.1). We will replace $\boldsymbol{u}_h^n$ on the left-hand side of (2.2) by an approximation to the Leray projection $\mathcal{P}\boldsymbol{u}_h^n$. The resulting scheme is a finite-element version of classical projection methods of Orszag et al [24] and Karniadakis et al [17], which incorporate the curl-curl of velocity in the boundary condition for pressure (see (1.9)). We use backward-Euler time differencing to get a scheme tractable to analysis.

It turns out that we can elegantly compute a projection of $\mathcal{P}\boldsymbol{u}_h^n$ into $X_{0,h}$ using the H_0^1 inner product $\langle \nabla \boldsymbol{u}, \nabla \boldsymbol{v} \rangle$. The identity (see [20, Lemma 1])

$$\Delta \mathcal{P}\boldsymbol{u} = \Delta \boldsymbol{u} - \nabla \nabla \cdot \boldsymbol{u} = -\nabla \times \nabla \times \boldsymbol{u} \qquad (3.2)$$

is valid for all $\boldsymbol{u} \in L^2(\Omega, \mathbb{R}^N)$, and implies that given any $\boldsymbol{u}_h, \boldsymbol{v}_h \in X_{0,h}$,

$$\langle \nabla \mathcal{P}\boldsymbol{u}_h, \nabla \boldsymbol{v}_h \rangle = -\langle \Delta \mathcal{P}\boldsymbol{u}_h, \boldsymbol{v}_h \rangle = \langle \nabla \times \boldsymbol{u}_h, \nabla \times \boldsymbol{v}_h \rangle.$$

Thus we get the following finite-element scheme with divergence suppression:

(i) Given $\boldsymbol{u}_h^n \in X_{0,h}$, find $\boldsymbol{u}_h^{n,*} \in X_{0,h}$ (the H_0^1 projection of $\mathcal{P}\boldsymbol{u}_h^n$) so that

$$\langle \nabla \boldsymbol{u}_h^{n,*}, \nabla \boldsymbol{v}_h \rangle = \langle \nabla \times \boldsymbol{u}_h^n, \nabla \times \boldsymbol{v}_h \rangle \qquad (3.3)$$

for all $\boldsymbol{v}_h \in X_{0,h}$.

(ii) Determine the pressure $p_h^n \in Y_h$ by requiring that for all $q_h \in Y_h$,

$$\langle \nabla p_h^n, \nabla q_h \rangle = \langle \boldsymbol{f}^n - \boldsymbol{u}_h^n \cdot \nabla \boldsymbol{u}_h^n, \nabla q_h \rangle + \nu \langle \nabla \times \boldsymbol{u}_h^n, \boldsymbol{n} \times \nabla q_h \rangle_\Gamma. \tag{3.4}$$

(iii) Update the velocity by finding $\boldsymbol{u}_h^{n+1} \in X_{0,h}$ so that for all $\boldsymbol{v}_h \in X_{0,h}$,

$$\left\langle \frac{\nabla \boldsymbol{u}_h^{n+1} - \nabla \boldsymbol{u}_h^{n,*}}{\Delta t}, \nabla \boldsymbol{v}_h \right\rangle + \nu \langle \Delta \boldsymbol{u}_h^{n+1}, \Delta \boldsymbol{v}_h \rangle = \langle \nabla p_h^n - \boldsymbol{f}^n + \boldsymbol{u}_h^n \cdot \nabla \boldsymbol{u}_h^n, \Delta \boldsymbol{v}_h \rangle \tag{3.5}$$

for all $q_h \in Y_h$ and $\boldsymbol{v}_h \in X_{0,h}$. Of course, one can avoid the expense of computing $\boldsymbol{u}_h^{n,*}$ by substituting (3.3) directly in (3.5).

We remark that since we know UNSE is well-posed, we can regard the approximate projection step (i) as a supplementary measure to suppress divergence errors; it is not necessary to maintain consistency. To save expense in related projection methods, a projection could be performed only once every several time steps.

3.2 Stability theorem

Here we establish a stability theorem for the C^1 finite element schemes (3.3)–(3.5). Similar to the proof of stability in [20] for the scheme (2.1)–(2.2) without a projection step, the main ingredient is the estimate on Stokes pressure in Theorem 1.1, thus the theorem is restricted to domains with C^3 boundary.

Theorem 3.1 *Assume that Ω is a bounded domain in $\mathbb{R}^N$ ($N = 2, 3$) with C^3 boundary. Then for any $M_0, \nu > 0$, there exist positive constants T_* and C_* with the following property. Suppose $Y_h \subset H^1(\Omega)$, $\boldsymbol{u}_h^0 \in X_{0,h} \subset H^2 \cap H_0^1(\Omega, \mathbb{R}^N)$, $\boldsymbol{f} \in C^1([0,T], L^2(\Omega, \mathbb{R}^N))$ for some $T > 0$, and suppose $0 < n\Delta t \leq \min(T, T_*)$ and*

$$\|\nabla \boldsymbol{u}_h^0\|^2 + \nu \Delta t \|\Delta \boldsymbol{u}_h^0\|^2 + \sum_{k=0}^n \|\boldsymbol{f}^k\|^2 \Delta t \leq M_0. \tag{3.6}$$

Then the solution to the finite element scheme (3.3)–(3.5) satisfies

$$\sup_{0 \leq k \leq n} \|\nabla \boldsymbol{u}_h^k\|^2 + \sum_{k=0}^n (\|\Delta \boldsymbol{u}_h^k\|^2 + \|\nabla p_h^k\|^2) \Delta t \leq C_*, \tag{3.7}$$

$$\sum_{k=0}^n \|\nabla \cdot \boldsymbol{u}_h^n\|^2 \Delta t \leq C_* \Delta t. \tag{3.8}$$

Proof (1) First, we rewrite (3.4) using (1.8) as

$$\langle \nabla p_h^n, \nabla q_h \rangle = \langle \boldsymbol{f}(t_n) - \boldsymbol{u}_h^n \cdot \nabla \boldsymbol{u}_h^n, \nabla q_h \rangle + \nu \langle \nabla p_{\mathrm{s}}(\boldsymbol{u}_h^n), \nabla q_h \rangle, \tag{3.9}$$

where $p_{\mathrm{s}}(\boldsymbol{u}_h^n)$ is the Stokes pressure associated with $\boldsymbol{u}_h^n$. Taking $q_h = p_h^n$, we get

$$\|\nabla p_h^n\| \leq \|\boldsymbol{f}(t_n) - \boldsymbol{u}_h^n \cdot \nabla \boldsymbol{u}_h^n\| + \nu \|\nabla p_{\mathrm{s}}(\boldsymbol{u}_h^n)\|. \tag{3.10}$$

Note

$$\langle \nabla \boldsymbol{u}_h^{n+1} - \nabla \boldsymbol{u}_h^{n,*}, \nabla \boldsymbol{v}_h \rangle = \langle \nabla \times \boldsymbol{u}_h^{n+1} - \nabla \times \boldsymbol{u}_h^n, \nabla \times \boldsymbol{v}_h \rangle + \langle \nabla \cdot \boldsymbol{u}_h^{n+1}, \nabla \cdot \boldsymbol{v}_h \rangle. \tag{3.11}$$

Now, let $\boldsymbol{v}_h = \boldsymbol{u}_h^{n+1}$ in (3.5) and use (3.11) and (3.10). We get

$$\frac{1}{2\Delta t}(\|\nabla \boldsymbol{u}_h^{n+1}\|^2 - \|\nabla \boldsymbol{u}_h^n\|^2 + \|\nabla \times \boldsymbol{u}_h^{n+1} - \nabla \times \boldsymbol{u}_h^n\|^2)$$
$$+ \frac{1}{2\Delta t}(\|\nabla \cdot \boldsymbol{u}_h^{n+1}\|^2 + \|\nabla \cdot \boldsymbol{u}_h^n\|^2) + \nu\|\Delta \boldsymbol{u}_h^{n+1}\|^2$$
$$\leq \|\Delta \boldsymbol{u}_h^{n+1}\|(2\|\boldsymbol{f}(t_n) - \boldsymbol{u}_h^n \cdot \nabla \boldsymbol{u}_h^n\| + \nu\|\nabla p_s(\boldsymbol{u}_h^n)\|)$$
$$\leq \frac{\varepsilon_1}{2}\|\Delta \boldsymbol{u}_h^{n+1}\|^2 + \frac{2}{\varepsilon_1}\|\boldsymbol{f}(t_n) - \boldsymbol{u}_h^n \cdot \nabla \boldsymbol{u}_h^n\|^2 + \frac{\nu}{2}(\|\Delta \boldsymbol{u}_h^{n+1}\|^2 + \|\nabla p_s(\boldsymbol{u}_h^n)\|^2)$$

for any $\varepsilon_1 > 0$. This gives

$$\frac{1}{\Delta t}(\|\nabla \boldsymbol{u}_h^{n+1}\|^2 - \|\nabla \boldsymbol{u}_h^n\|^2) + \frac{1}{\Delta t}\|\nabla \cdot \boldsymbol{u}^n\|^2 + (\nu - \varepsilon_1)\|\Delta \boldsymbol{u}_h^{n+1}\|^2$$
$$\leq \frac{8}{\varepsilon_1}(\|\boldsymbol{f}(t_n)\|^2 + \|\boldsymbol{u}_h^n \cdot \nabla \boldsymbol{u}_h^n\|^2) + \nu\|\nabla p_s(\boldsymbol{u}_h^n)\|^2. \tag{3.12}$$

Fix any β with $\frac{1}{2} < \beta < 1$. Using Theorem 1.1 with $\boldsymbol{u} = \boldsymbol{u}_h^n$, one obtains

$$\frac{1}{\Delta t}(\|\nabla \boldsymbol{u}_h^{n+1}\|^2 - \|\nabla \boldsymbol{u}_h^n\|^2) + \frac{1}{\Delta t}\|\nabla \cdot \boldsymbol{u}^n\|^2$$
$$+ (\nu - \varepsilon_1)(\|\Delta \boldsymbol{u}_h^{n+1}\|^2 - \|\Delta \boldsymbol{u}_h^n\|^2) + (\nu - \varepsilon_1 - \nu\beta)\|\Delta \boldsymbol{u}_h^n\|^2$$
$$\leq \frac{8}{\varepsilon_1}(\|\boldsymbol{f}(t_n)\|^2 + \|\boldsymbol{u}_h^n \cdot \nabla \boldsymbol{u}_h^n\|^2) + \nu C_\beta\|\nabla \boldsymbol{u}_h^n\|^2. \tag{3.13}$$

(2) The pressure no longer appears at this point. Now, as in [20], we use inequalities of Ladyzhenskaya to obtain, for all $g \in H^1(\Omega)$,

$$\|g\|_{L^4}^2 \leq C\|g\|_{L^2}\|g\|_{H^1}, \qquad\qquad N = 2, \tag{3.14}$$

$$\|g\|_{L^3}^2 \leq \|g\|_{L^2}^{\frac{2}{3}}\|g\|_{L^4}^{\frac{4}{3}} \leq C\|g\|_{L^2}\|g\|_{H^1}, \quad N = 3. \tag{3.15}$$

Since $H^1(\Omega) \subset L^4$ and L^6, for all $\boldsymbol{u} \in H^2 \cap H_0^1(\Omega, \mathbb{R}^N)$ we have

$$\|\boldsymbol{u} \cdot \nabla \boldsymbol{u}\|^2 \leq \begin{cases} \|\boldsymbol{u}\|_{L^4}^2\|\nabla \boldsymbol{u}\|_{L^4}^2 \leq C\|\boldsymbol{u}\|_{L^2}\|\nabla \boldsymbol{u}\|_{L^2}^2\|\nabla \boldsymbol{u}\|_{H^1}, & N = 2, \\ \|\boldsymbol{u}\|_{L^6}^2\|\nabla \boldsymbol{u}\|_{L^3}^2 \leq C\|\nabla \boldsymbol{u}\|_{L^2}^3\|\nabla \boldsymbol{u}\|_{H^1}, & N = 3. \end{cases} \tag{3.16}$$

With $\boldsymbol{u} = \boldsymbol{u}_h^n$, using the elliptic regularity estimate $\|\boldsymbol{u}_h^n\|_{H^2} \leq C\|\Delta \boldsymbol{u}_h^n\|$, we find that for any $\varepsilon_2 > 0$ there exists $C > 0$ such that

$$\|\boldsymbol{u}_h^n \cdot \nabla \boldsymbol{u}_h^n\|^2 \leq C\|\nabla \boldsymbol{u}_h^n\|^3\|\Delta \boldsymbol{u}_h^n\| \leq \varepsilon_2\|\Delta \boldsymbol{u}_h^n\|^2 + \frac{C}{\varepsilon_2}\|\nabla \boldsymbol{u}_h^n\|^6. \tag{3.17}$$

Using this in (3.13) and taking $\varepsilon_1, \varepsilon_2 > 0$ small, we get, for some $\varepsilon > 0$,

$$\frac{1}{\Delta t}(\|\nabla \boldsymbol{u}_h^{n+1}\|^2 - \|\nabla \boldsymbol{u}_h^n\|^2) + \frac{1}{\Delta t}\|\nabla \cdot \boldsymbol{u}^n\|^2 + (\nu - \varepsilon_1)(\|\Delta \boldsymbol{u}_h^{n+1}\|^2 - \|\Delta \boldsymbol{u}_h^n\|^2) + \varepsilon\|\Delta \boldsymbol{u}_h^n\|^2$$
$$\leq \frac{8}{\varepsilon_1}\|\boldsymbol{f}(t_n)\|^2 + \frac{8C}{\varepsilon_1\varepsilon_2}\|\nabla \boldsymbol{u}_h^n\|^6 + \nu C_\beta\|\nabla \boldsymbol{u}_h^n\|^2. \tag{3.18}$$

(3) The last step is a discrete Gronwall-type argument. (A general result of this type of argument is formulated in [21].) Put $b_n = \|\boldsymbol{f}(t_n)\|^2$ and

$$z_n = \|\nabla \boldsymbol{u}_h^n\|^2 + (\nu - \varepsilon_1)\Delta t\|\Delta \boldsymbol{u}_h^n\|^2, \quad w_n = \varepsilon\|\Delta \boldsymbol{u}_h^n\|^2 + \frac{1}{\Delta t}\|\nabla \cdot \boldsymbol{u}_h^n\|^2. \tag{3.19}$$

Then by (3.18), we get $z_{n+1} + w_n\Delta t \leq z_n + C\Delta t(b_n + z_n + z_n^3)$. Summing from 0 to $n-1$ and using (3.6) yields

$$z_n + \sum_{k=0}^{n-1} w_k\Delta t \leq CM_0 + C\Delta t \sum_{k=0}^{n-1}(z_k + z_k^3) =: y_n. \tag{3.20}$$

Then y_n increases with n and $y_{n+1} - y_n = C\Delta t(z_n + z_n^3) \leq C\Delta t(y_n + y_n^3)$. Let $F(y) = \ln\left(\frac{y}{\sqrt{1+y^2}}\right)$ so that $F'(y) = (y+y^3)^{-1}$. Then on $(0,\infty)$, F is negative, increasing and concave, and we have

$$F(y_{n+1}) - F(y_n) \leq F'(y_n)(y_{n+1} - y_n) = \frac{y_{n+1} - y_n}{y_n + y_n^3} \leq C\Delta t, \tag{3.21}$$

hence $F(y_n) \leq F(y_0) + Cn\Delta t = F(CM_0) + Cn\Delta t$. Choosing $T_* > 0$ so that $C_* := F(CM_0) + CT_* < 0$, we deduce that for $n\Delta t \leq T_*$ we have $y_n \leq F^{-1}(C_*)$, and this with (3.20) yields (3.7) and (3.8).

Remark 3.1 If nonlinear terms were absent, T_* could be fixed arbitrarily — we get unconditional stability in the case of the linear Stokes equation. In general, T_* is independent of the spatial discretization, but is limited in size by nonlinearity, even in two dimensions when solutions exist globally in time. We apply the same remarks to the error estimates proved in the next section for the scheme (2.1), (2.2) without a projection step. Also, we point out that although the data $\boldsymbol{u}_h^0$ are required to be in H^2, the weak dependence of the bound (3.6) on $\Delta\boldsymbol{u}_h^0$ allows one to approximate any data $\boldsymbol{u}_{\mathrm{in}} \in H_0^1(\Omega, \mathbb{R}^N)$ with zero divergence by a suitable $\boldsymbol{u}_h^0 \in X_{0,h}$. In [20], a similar smoothing step was used to prove the existence and uniqueness of the solution of UNSE with any initial data $\boldsymbol{u}_{\mathrm{in}} \in H_0^1(\Omega, \mathbb{R}^N)$, having the regularity

$$\boldsymbol{u} \in L^2(0, T_*; H^2(\Omega, \mathbb{R}^N)) \cap H^1(0, T_*; L^2(\Omega, \mathbb{R}^N)). \tag{3.22}$$

4 Practical Issues

4.1 Non-homogeneous boundary conditions

We handle non-homogeneous boundary conditions for the velocity in the way described in [20]. Suppose that the no-slip boundary condition (1.3) is replaced by

$$\boldsymbol{u} = \boldsymbol{g} \quad \text{on } \Gamma. \tag{4.1}$$

The boundary data $\boldsymbol{g}$ is required to satisfy the compatibility condition

$$\int_\Gamma \boldsymbol{n} \cdot \boldsymbol{g} = 0 \quad \text{for } t > 0.$$

In [20] we proved unconditional stability and convergence of the following time-discrete scheme for the NSE equations (1.1)–(1.2) and (4.1), under appropriate conditions on regularity and initial compatibility for the data. Given $\boldsymbol{u}^n \in H^2(\Omega, \mathbb{R}^N)$, we determine $\nabla p^n \in L^2(\Omega, \mathbb{R}^N)$ so that for all $q \in H^1(\Omega)$,

$$\langle \nabla p^n, \nabla q \rangle = \langle \boldsymbol{f}^n - \boldsymbol{u}^n \cdot \nabla \boldsymbol{u}^n, \nabla q \rangle + \nu \langle \nabla \times \boldsymbol{u}^n, \boldsymbol{n} \times \nabla q \rangle_\Gamma - \left\langle \frac{\boldsymbol{n} \cdot (\boldsymbol{g}^{n+1} - \boldsymbol{g}^n)}{\Delta t}, q \right\rangle_\Gamma, \tag{4.2}$$

then determine $\boldsymbol{u}^{n+1} \in H^2(\Omega, \mathbb{R}^N)$ from the boundary value problem

$$\frac{\boldsymbol{u}^{n+1} - \boldsymbol{u}^n}{\Delta t} - \nu \Delta \boldsymbol{u}^{n+1} = \boldsymbol{f}^n - \boldsymbol{u}^n \cdot \nabla \boldsymbol{u}^n - \nabla p^n, \tag{4.3}$$

$$\boldsymbol{u}^{n+1}|_\Gamma = \boldsymbol{g}^{n+1}. \tag{4.4}$$

To incorporate divergence suppression, we want to approximate a divergence-free projection $\boldsymbol{u}^{n,*}$ to $\boldsymbol{u}^n$ that preserves the normal component, with $\boldsymbol{n} \cdot \boldsymbol{u}^{n,*} = \boldsymbol{n} \cdot \boldsymbol{u}^n$ on Γ. In practice, it is convenient to use L^2-projection for this rather than the H_0^1-projection of the previous section. Given $\boldsymbol{u}_h^n$, we determine an approximation $\boldsymbol{u}_h^{n,*}$ to $\mathcal{P}\boldsymbol{u}_h^n$ in terms of $\phi_h^n \in Y_h$ so that

$$\boldsymbol{u}_h^{n,*} = \boldsymbol{u}_h^n - \nabla \phi_h^n, \quad \langle \nabla \phi_h^n, \nabla q_h \rangle = -\langle \nabla \cdot \boldsymbol{u}_h^n, q_h \rangle, \quad \forall q_h \in Y_h. \tag{4.5}$$

To save computation, we combine the determination of ϕ_h^n and p_h^n and simply compute $\widehat{p}_h^n = p_h^n + \frac{\phi_h^n}{\Delta t}$. Thus, in the first step of a fully discrete finite-element scheme, we determine $\widehat{p}_h^n \in Y_h$ so that for all $q_h \in Y_h$,

$$\langle \nabla \widehat{p}_h^n, \nabla q_h \rangle = \langle \boldsymbol{f}^n - \boldsymbol{u}_h^n \cdot \nabla \boldsymbol{u}_h^n, \nabla q_h \rangle + \nu \langle \nabla \times \boldsymbol{u}_h^n, \boldsymbol{n} \times \nabla q_h \rangle_\Gamma$$
$$- \left\langle \frac{\boldsymbol{n} \cdot (\boldsymbol{g}^{n+1} - \boldsymbol{g}^n)}{\Delta t}, q_h \right\rangle_\Gamma - \frac{1}{\Delta t} \langle \nabla \cdot \boldsymbol{u}_h^n, q_h \rangle. \tag{4.6}$$

To update velocity, we look for $\boldsymbol{u}_h^n$ in a space of C^1 finite elements $X_h \supseteq X_{0,h}$, with $X_h \subset H^2(\Omega, \mathbb{R}^N)$. Using ∂_τ to denote tangential derivatives, we require

$$\boldsymbol{u}_h^{n+1} = \boldsymbol{g}(t_{n+1}), \quad \partial_\tau \boldsymbol{u}_h^{n+1} = \partial_\tau \boldsymbol{g}(t_{n+1}) \tag{4.7}$$

for all corresponding boundary degrees of freedom (DOF, i.e., those parameters which uniquely define a function in the space X_h). Once the DOF at the boundary are taken care of, the DOF at interior points of the triangulated domain are determined by solving the following equation for any $\boldsymbol{v}_h \in X_{0,h}$,

$$\left\langle \frac{\boldsymbol{u}_h^{n+1} - \boldsymbol{u}_h^n}{\Delta t}, \Delta \boldsymbol{v}_h \right\rangle - \nu \langle \Delta \boldsymbol{u}_h^{n+1}, \Delta \boldsymbol{v}_h \rangle = \langle \boldsymbol{f}^n - \boldsymbol{u}_h^n \cdot \nabla \boldsymbol{u}_h^n - \nabla \widehat{p}_h^n, \Delta \boldsymbol{v}_h \rangle. \tag{4.8}$$

4.2 Obtuse corners, C^1 finite elements and recycling

It is well-known that even for the linear Poisson equation with zero boundary condition, the exact solution in an L-shaped domain may fail to be in $H^2(\Omega)$, even though the forcing term is C^∞ and zero near the corners — a simple example is based on a cut-off of the function written in polar coordinates as

$$u(r, \theta) = r^{\frac{2}{3}} \sin\left(\frac{2\theta}{3}\right), \tag{4.9}$$

which is harmonic and satisfies $u(r, 0) = 0 = u(r, \frac{3\pi}{2})$. For the Navier-Stokes equations, similar singularities are known to occur and may be responsible for poor performance of C^1 finite element methods in problems in domains with re-entrant corners, such as flow over a backward facing step.

A practical approach that we have used to recover reasonable results using C^1 finite elements in this situation is to expand the C^1 finite element space for velocity, by "recycling" some

basis functions associated with tangential derivatives at the corner, whose associated degrees of freedom are otherwise discarded when imposing the no-slip condition. These recycled C^1 basis functions are then crudely truncated to make them only C^0. This will allow jumps in directional derivatives at the corner.

To be more specific, we will illustrate the problem in 2D with a particular kind of C^1 finite element that we have used in our computation, namely, the Fraeijs de Veubeke-Sander (FVS) type C^1 finite elements (see [6, Exercises 6.1.5] and [8, 19]). It will be evident that this recycling technique does not depend on a detailed understanding of corner singularities, and can be extended to other C^1 finite elements in both $\mathbb{R}^2$ and $\mathbb{R}^3$. FVS elements are piecewise 3rd-order polynomials with 16 degrees of freedom in each FVS element. See Figure 1 for a descriptive diagram — the arrows stand for evaluating directional derivatives, and the dots mean taking values at the associated points.
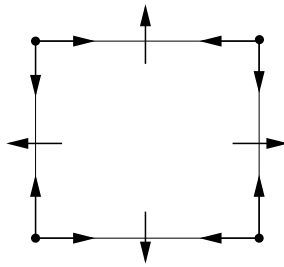

Figure 1 FVS finite element.

If we have an obtuse corner, we need to put three elements (or rectangles) around the corner. See Figure 2 for an illustration. For globally C^1 functions in the finite-element space, there are three degrees of freedom at the vertex of the corner: one value and two directional derivatives. The problem comes from the directional derivatives, which we will denote by a and b for the horizontal and vertical derivatives, respectively. The basis function associated with a and b are denoted by ϕ_a and ϕ_b, which are supported in the rectangles I, II and III in Figure 2. Any component of $\boldsymbol{u}_h = (u_h, v_h)$, say, u_h, is represented as

$$u_h = a\phi_a + b\phi_b + \cdots. \tag{4.10}$$

In Figure 2, we intentionally use a_i and b_i $(i = 1, 2, 3)$ to denote the a and b evaluated separately in different rectangles at the vertex since ϕ_a and ϕ_b are supported in all three rectangles.
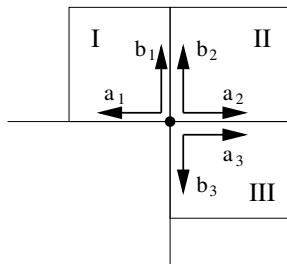

Figure 2 FEs around the corner.

(1) No-slip boundary values. No-slip boundary conditions require $a_1 = b_3 = 0$. To use C^1 finite elements in the standard way, since derivatives of ϕ_a and ϕ_b are continuous, one must set $a_i = b_i = 0$ for $i = 1, 2, 3$. Hence the first two terms in (4.10) drop, and ϕ_a and ϕ_b are never used. As reported below in Section 5, this leads to poor results for flow over a backward facing step.

The way to "recycle" ϕ_a and ϕ_b and improve the situation is very simple: We truncate ϕ_a so that it is zero in rectangle I, and remains unchanged in rectangles II and III. We call it $\widetilde{\phi}_a$. We truncate ϕ_b so that it is zero in rectangle III, and remains unchanged in rectangles I and II. We call it $\widetilde{\phi}_b$. Then, we put $\widetilde{\phi}_a$ and $\widetilde{\phi}_b$ back into (4.10) (with a tilde on top) so that now the a represents the x derivatives along the edge between rectangles II and III; b represents the the y derivatives along the edge between rectangles I and II.

If we recycle basis elements in this way, using $U_{0,h}$ to denote the original FVS finite element space, we get an expanded FVS finite-element space

$$\widetilde{U}_{0,h} = U_{0,h} \oplus \operatorname{span}\{\widetilde{\phi}_a, \widetilde{\phi}_b\} \tag{4.11}$$

and a new finite-element space for velocity,

$$\widetilde{X}_{0,h} = \widetilde{U}_{0,h} \times \widetilde{U}_{0,h}. \tag{4.12}$$

We can then use the same equations, say, (4.6) and (4.8) to solve for $\widehat{p}_h^n$ and velocity $\boldsymbol{u}_h^{n+1}$. The space Y_h remains unchanged. However, terms containing second derivatives of $\boldsymbol{u}_h^n$, $\boldsymbol{u}_h^{n+1}$ and $\boldsymbol{v}_h$ are now being computed and integrated element-wise. For example, the term $\langle \boldsymbol{u}_h^n \cdot \nabla \boldsymbol{u}_h^n, \Delta \boldsymbol{v}_h \rangle_\Omega$ is now replaced by $\sum_k \langle \boldsymbol{u}_h^n \cdot \nabla \boldsymbol{u}_h^n, \Delta \boldsymbol{v}_h \rangle_{\mathcal{T}_k}$, where $\{\mathcal{T}_k\}$ is the triangulation of Ω associated with $\widetilde{X}_{0,h}$. (We do not add jump terms on the element boundaries. Numerical experiments that we performed including such jump terms showed no essential difference.) Note that the matrix that we need to invert in order to solve for $\boldsymbol{u}_h^{n+1}$ remains symmetric positive definite when corners are handled in this way.

(2) Non-homogeneous boundary values. In the case that the boundary data $\boldsymbol{g} \neq 0$, the space X_h is modified as follows: we use the traditional approach to treat the x-derivative in rectangle I and y-derivatives in rectangle III. The other derivatives at the corner in rectangle I and III, and the two derivatives at the corner in rectangle II are set to be unknown and to be determined from momentum equations (4.21). So, for example, for the x-component of $\boldsymbol{u}_h = (u_h, v_h)$, suppose that g_1 is the x-component of $\boldsymbol{g}$,

$$u_h = (\partial_x g_1)\phi_a + b\phi_b + \cdots \quad \text{in rectangle I}, \tag{4.13}$$

$$u_h = a\phi_a + b\phi_b + \cdots \quad \text{in rectangle II}, \tag{4.14}$$

$$u_h = a\phi_a + (\partial_y g_1)\phi_b + \cdots \quad \text{in rectangle III}, \tag{4.15}$$

where a and b are unknowns to be determined from the momentum equation as before, after we enlarge the test function space $X_{0,h} \subset H^2 \cap H_0^1(\Omega, \mathbb{R}^N)$ to (4.12). The information from $\partial_\tau \boldsymbol{g}$ has been fully taken care of and the stiffness and mass matrices from the momentum equation are still symmetric positive definite.

A different approach of handling reentrant corners has been introduced by Soane and Rostamian [26], who use weighted variational problems to determine the Stokes pressure.

4.3 Higher-order time integration

We get a basic 2nd-order scheme by discretizing the momentum equation using 2nd-order backward differentiation formula for the viscosity and 2nd-order extrapolation formulas for explicit treatment of pressure and convection terms. Using the notation

$$\boldsymbol{h}^n = \boldsymbol{u}^n \cdot \nabla \boldsymbol{u}^n, \tag{4.16}$$

we get the following semi-discrete BD2/X2 scheme:

$$\frac{3\boldsymbol{u}^{n+1} - 4\boldsymbol{u}^n + \boldsymbol{u}^{n-1}}{2\Delta t} + 2(\nabla p^n + \boldsymbol{h}^n) - (\nabla p^{n-1} + \boldsymbol{h}^{n-1}) = \nu \Delta \boldsymbol{u}^{n+1} + \boldsymbol{f}^{n+1} \tag{4.17}$$

with $\boldsymbol{u}^{n+1} = 0$ on Γ. The pressure equation is (see [20] or (4.6))

$$\langle \nabla p^n, \nabla q \rangle = \langle \boldsymbol{f}^n - \boldsymbol{h}^n, \nabla q \rangle + \nu \langle \nabla \times \boldsymbol{u}^n, \boldsymbol{n} \times \nabla q \rangle_\Gamma - \langle \boldsymbol{n} \cdot \partial_t \boldsymbol{g}(t_n), q \rangle_\Gamma \tag{4.18}$$

for any $q \in H^1(\Omega)$. The divergence suppression we mentioned before can be easily incorporated into the above scheme, and we get the following fully discrete scheme (a finite-element variant of the projection methods of [17]):

$$\overline{\boldsymbol{u}}_h = -\frac{1}{2\Delta t}(4\boldsymbol{u}_h^n - \boldsymbol{u}_h^{n-1}) + (2\boldsymbol{h}_h^n - \boldsymbol{h}_h^{n-1}) - \boldsymbol{f}^{n+1}, \tag{4.19}$$

$$\langle \nabla \overline{P}_h, \nabla q_h \rangle = -\langle \overline{\boldsymbol{u}}_h, \nabla q_h \rangle + \nu \langle \nabla \times (2\boldsymbol{u}_h^n - \boldsymbol{u}_h^{n-1}), \boldsymbol{n} \times \nabla q_h \rangle_\Gamma$$
$$- \frac{3}{2\Delta t}\langle \boldsymbol{n} \cdot \boldsymbol{g}^{n+1}, q_h \rangle_\Gamma, \quad \forall q_h \in Y_h, \tag{4.20}$$

$$\left\langle \frac{3\boldsymbol{u}_h^{n+1}}{2\Delta t}, \Delta \boldsymbol{v}_h \right\rangle - \nu \langle \Delta \boldsymbol{u}_h^{n+1}, \Delta \boldsymbol{v}_h \rangle = -\langle \overline{\boldsymbol{u}}_h + \nabla \overline{P}_h, \Delta \boldsymbol{v}_h \rangle, \quad \forall \boldsymbol{v}_h \in X_{0,h}, \tag{4.21}$$

where $\boldsymbol{h}_h^n = \boldsymbol{u}_h^n \cdot \nabla \boldsymbol{u}_h^n$. On the boundary Γ, we assign the associated degrees of freedom of $\boldsymbol{u}_h^{n+1}$ equal to either $\boldsymbol{g}^{n+1}$ or tangential derivative of $\boldsymbol{g}^{n+1}$. Note that there is only one pressure-like quantity computed in each time step.

4.4 How to solve for the pressure

We want to briefly indicate how we solve the pressure equation (2.1), because typically one has to deal with a singular mass matrix $A = (\langle \nabla \phi_i, \nabla \phi_j \rangle)$, where $\{\phi_i\}_{i=1}^D$ is a basis for the finite-element pressure space Y_h. Here D is the number of degrees of freedom in Y_h. If we write $p_h^n = \sum_i p_i \phi_i$ and

$$b_i = \langle \boldsymbol{f}^n - \boldsymbol{u}_h^n \cdot \nabla \boldsymbol{u}_h^n, \nabla \phi_i \rangle + \nu \langle \nabla \times \boldsymbol{u}_h^n, \boldsymbol{n} \times \nabla \phi_i \rangle_\Gamma, \tag{4.22}$$

the pressure equation (2.1) is equivalent to the system of equations

$$A\boldsymbol{p} = \boldsymbol{b} \tag{4.23}$$

with $\boldsymbol{p} = (p_i)$ and $\boldsymbol{b} = (b_i)$. If $A\boldsymbol{p} = 0$ for some $\boldsymbol{p} \in \mathbb{R}^D$, then correspondingly, $\boldsymbol{p}^{\mathrm{T}} A \boldsymbol{p} = \int_\Omega |\nabla p_h^n|^2 = 0$ and hence p_h^n must be a constant in Ω. Thus A is singular if and only if the constant $1 \in Y_h$, which is typical. A solution of (4.23) always exists, however, since if $1 = \sum_i c_i \phi_i \in Y_h$ then $\boldsymbol{b}$ in (4.22) naturally satisfies the solvability condition $\boldsymbol{c}^{\mathrm{T}} \boldsymbol{b} = 0$.

What we can do to compute a solution is simply remove some single basis element ϕ_j from the set $\{\phi_i\}_{i=1}^D$, such that if $1 = \sum_i c_i \phi_i$ then $c_j \neq 0$. In practice, this usually means deleting a single basis element ϕ_j, such that the value p_j corresponds to a nodal value of p_h^n. Then it follows $1 \notin \widehat{Y}_h = \mathrm{span}\{\phi_i : i \neq j\}$. Hence we can solve (4.23) by deleting the jth row and column from matrix A, and the jth row from $\boldsymbol{b}$, solving the resulting $(D-1) \times (D-1)$ (symmetric, positive definite) system, and setting $p_j = 0$ afterward.

5 Numerical Tests

In this section, we document the numerical performance of the C^1 finite element schemes described in this paper. We (i) check the stability and spatial accuracy of our schemes, and (ii) apply our methods to benchmark problems involving driven cavity flow and flow over a backward-facing step.

For C^1 finite element computations, we use Fraeijs de Veubeke-Sander (FVS) type elements, which are piecewise 3rd-order polynomials with 16 degrees of freedom in each FVS quadrilateral. See Figure 1 and the discussion in Section 4.2.

We will report results for the following smooth test problem. We take the domain to be $[-1, 1] \times [-1, 1]$ and let the exact solution be

$$
\begin{pmatrix} u(x,y,t) \\ v(x,y,t) \\ p(x,y,t) \end{pmatrix} = \begin{pmatrix} g(t) \cos^2(\frac{\pi x}{2}) \sin(\pi y) \\ -g(t) \sin(\pi x) \cos^2(\frac{\pi y}{2}) \\ g(t) \cos(\frac{\pi x}{2}) \sin(\frac{\pi y}{2}) \end{pmatrix},
\tag{5.1}
$$

where $g(t) = \cos(t)$. The forcing term $\boldsymbol{f}$ is chosen so that this is a solution of NSE. We take $\nu = 1$.

5.1 Stability checks

We studied the stability of the schemes treated in Theorems 2.1 and 3.1, and the schemes (4.17)–(4.18) and (4.19)–(4.21) which are formally second-order accurate in time. We fixed a 16×16 finite-element mesh and integrated to $T = 10000$ by using time steps Δt as large as 8. For the exact solution in (5.1), the errors of velocity and pressure remained bounded, indicating that these schemes are stable for time steps large of order $O(1)$ when $\nu = 1$. In general, the maximum time step for nonlinear stability appears to depend on viscosity and nonlinearity in a problem-dependent way; when viscosity is small, the stability of these implicit-explicit methods is limited by the explicit treatment of the nonlinear terms. See Section 5.3 for examples.

5.2 Spatial accuracy checks

In Table 1, we study the spatial accuracy for the projection method (4.19)–(4.21) by using FVS elements. The main quantity tabulated is $-\log_{10} E$ where E is the quantity listed in the left-hand column. (This indicates the number of essentially correct digits in E.) We have used a scheme formally second-order accurate in time and taken Δt small enough so that the error is mainly due to spatial discretization. In parentheses, we also list the local convergence rate α

for E, determined from the formula

$$\alpha = \frac{\log\left(\frac{E_k}{E_{k-1}}\right)}{\log\left(\frac{h_k}{h_{k-1}}\right)}. \tag{5.2}$$

Values of α in the first column of Table 1 are based on values of E for a larger h not shown. Essentially similar results were obtained for this test problem with the scheme (4.17)–(4.18) that does not involve a projection of velocity.

Table 1 Spatial accuracy check with FVS elements. $-\log_{10} E$ (and local order α) vs h. Scheme (4.19)–(4.21) with $\Delta t = \frac{h^2}{2}$, $\nu = 1$, $T = 2$.

$E \setminus h$	$\frac{2}{32}$	$\frac{2}{45}$	$\frac{2}{64}$	$\frac{2}{91}$
$\|p - p_h\|_\infty$	5.81 (4.39)	6.42 (4.14)	7.06 (4.18)	7.68 (4.09)
$\|u - u_h\|_\infty$	6.18 (4.0)	6.78 (3.99)	7.39 (4.0)	8.0 (3.99)
$\|\nabla \cdot \boldsymbol{u}_h\|_\infty$	4.45 (2.99)	4.89 (3.0)	5.35 (3.0)	5.81 (3.0)
$\|\widetilde{p} - p_h\|$	5.95 (3.94)	6.55 (4.08)	7.16 (3.99)	7.78 (4.04)
$\|\widetilde{u} - u_h\|$	6.26 (3.99)	6.86 (4.0)	7.47 (4.0)	8.08 (3.99)
$\|\nabla \cdot \boldsymbol{u}_h\|$	5.59 (3.63)	6.12 (3.58)	6.66 (3.54)	7.20 (3.52)
$\|\nabla(\widetilde{p} - p_h)\|$	4.28 (3.50)	4.80 (3.51)	5.33 (3.51)	5.87 (3.51)
$\|\nabla(\widetilde{u} - u_h)\|$	5.27 (3.61)	5.80 (3.58)	6.35 (3.56)	6.89 (3.54)
$\|\nabla(p - p_h)\|_\infty$	3.22 (2.93)	3.66 (2.97)	4.12 (2.98)	4.58 (3.0)
$\|\nabla(u - u_h)\|_\infty$	4.45 (2.99)	4.89 (3.0)	5.35 (3.0)	5.81 (3.0)

The tabulated L^2 errors compare the numerical solution with the interpolants $\widetilde{p}$ and $\widetilde{u}$ of the exact solution. For both velocity and pressure errors, Table 1 indicates that for this C^1 finite element scheme, the error of gradients is of order $O(h^3)$, the optimal rate achieved by the interpolation error $\nabla(u - \widetilde{u})$ with FVS elements. (In L^2-norm, the gradient of differences between the numerical solution and the interpolant is one-half order more accurate. This may be related to well-known superconvergence results for the difference between the numerical solution and a projection of the exact solution, for method-of-lines finite-element solutions of parabolic problems such as the heat equation.)

This result is consistent with the (time-integrated) error estimate $O(h^2)$ for the Laplacian of velocity from Theorem 2.1 for the Backward-Euler/Forward-Euler version of this scheme without projection in smooth domains. The $O(h^3)$ convergence rate indicated for the pressure gradient error is better, though, than the $O(h^2)$ rate that would be provided by the theorem for time-integrated error, were it applicable.

5.3 Driven cavity and backward-facing step tests

In this subsection, we test our finite element schemes for driven cavity flow (with $\mathrm{Re} = 1000$) and flow over a backward facing step (with $\mathrm{Re} = 100$ and 600).

For the driven cavity flow, we compute the flow in the domain $[0, 1] \times [0, 1]$ and start from rest, impulsively imposing horizontal velocity $u = 1$ on the top boundary for $t > 0$. Following [5], we plot the contours of vorticity with values $[-5, -4, -3, -2, -1, -0.5, 0, 0.5, 1, 2, 3]$. We also follow [18] to plot normalized velocity fields in order to visualize flow details near the corner. These plots also show the non-uniform mesh used. We refer to computational results of

[5, 18] for comparison. Although we use a rather coarse mesh, the vorticity contour plots agree quite well with [5].

For the backward-facing step, we use FVS finite elements to compute the flow in the domain

$$\Omega = [0, L] \times [-0.5, 0.5] \setminus [0, 0.5] \times [-0.5, 0]$$

with no-slip boundary conditions everywhere except at the inflow boundary $x = 0$ and the outflow boundary $x = L$. We take $L = 8$ when Re $= 100$, and take $L = 20$ when Re $= 600$. We start from rest and gradually increase the boundary velocity (u, v) to $(12y(1 - 2y), 0)$ at the inflow boundary and $(-3y^2 + \frac{3}{4}, 0)$ at the outflow boundary, with no net influx at each time. The time-dependent function we used for gradually increasing velocity is $\frac{1-\cos(\pi t)}{2}$ on $[0, 1]$. Once the velocity field is obtained, we use the streamline function in MATLAB to plot the streamlines. The mesh used is shown in Figure 3.
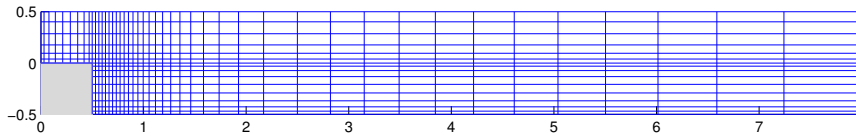

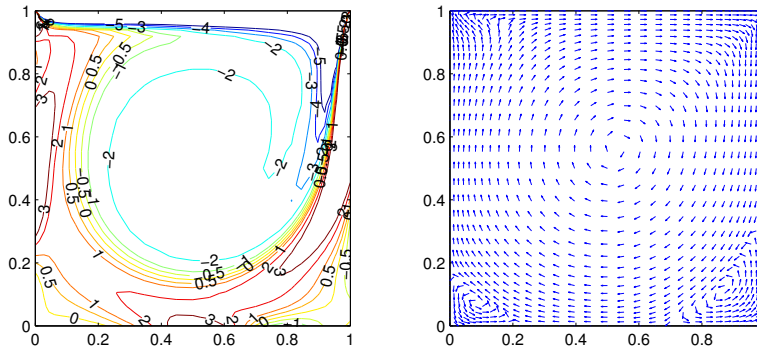Figure 3 Mesh used in backward facing step flow computation when Re $= 100$.

Figure 4 Driven cavity, Re $= 1000$. 32×32 C^1 FVS elements for each variable, $h_{\min} = 0.0131$. No recycling. Scheme (4.19)–(4.21), $\Delta t = 0.0075$, $T = 50$.

From Figure 5, we can see that a straight forward application of C^1 finite elements in domains with reentrant corner can lead to wrong results where continuity of derivatives across elements touching the reentrant corner is maintained. For those wrong results, we have tried to use finer grids and smaller time steps, but they are not very helpful. It seems that the problem is not due to under-resolution, because the computation works once we turn on the recycling. Figure 5 compares results with and without recycling at different times. It also shows the (approximately constant) flux $\int u_h(x, y)\mathrm{d}y$ integrated along vertical lines $x = $ const plotted against the distance x downstream from the inlet. Obviously the recycling techniques save the computation. The results for Re $= 600$ with recycling are shown in Figure 6. Even though we use a rather coarse mesh, the ratios between the size of the step (S) and the reattachment length and other characteristic lengths $(X_1, X_2, X_3$ as indicated in Figure 6) agree quite well with what is in the literature results [1, 18].
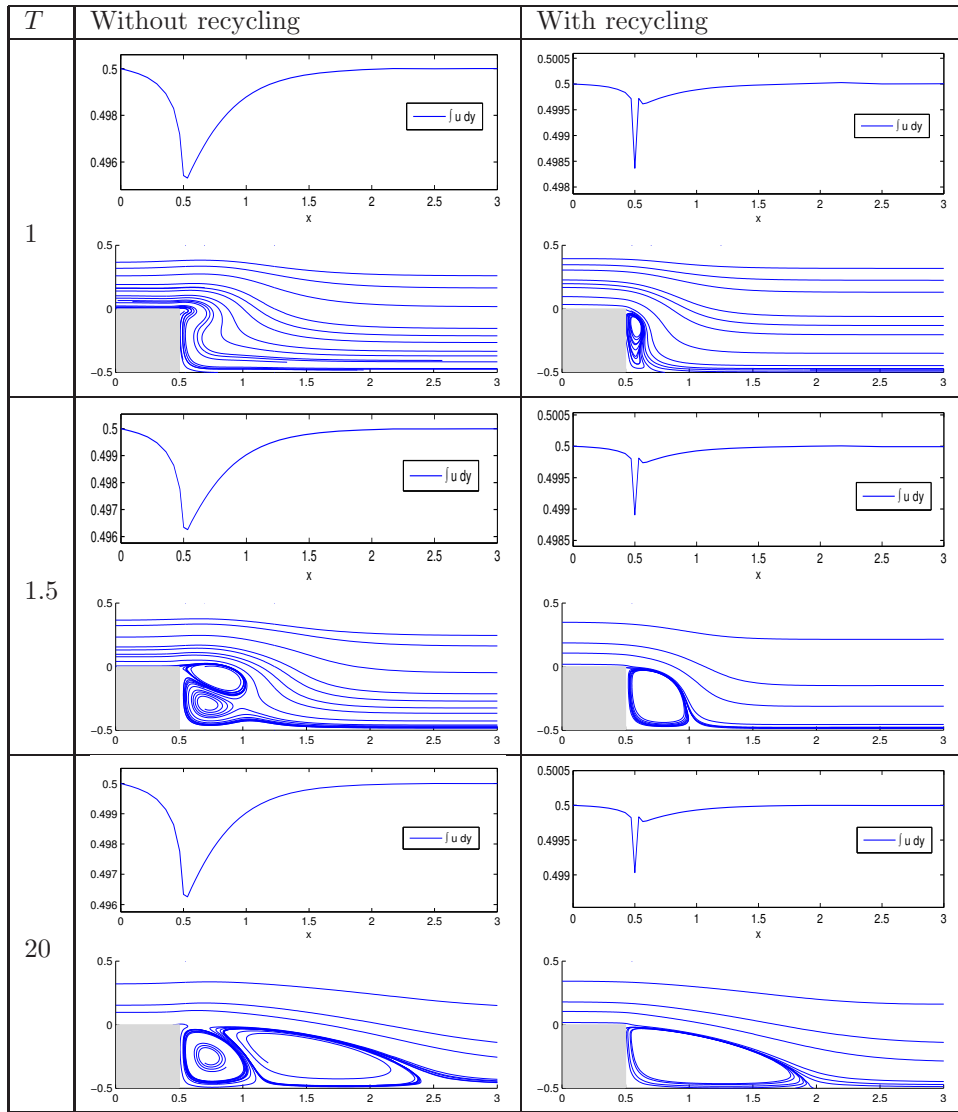
T	Without recycling	With recycling
1		
1.5		
20		

Figure 5 Backward facing step. Re $= 100$. Scheme (4.19)–(4.21) with recycling (right plots) and without recycling (left plots). 594 FVS elements for each variable. $h_{\min} = 0.0301$. $\Delta t = 0.006$. Flow at times $T = 1.002$, 1.5, 19.998. Above each streamline plot we plot the flux $\int u_h(x,y)\mathrm{d}y$ vs. x.
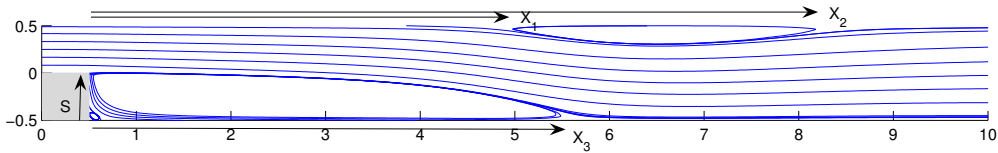

Figure 6 Backward facing step. Re $= 600$. Scheme (4.19)–(4.21) with recycling. 1107 FVS elements for each variable. $h_{\min} = 0.0301$. $\Delta t = 0.003$. $T = 120$. $\frac{X_1}{S} = 8.9$. $\frac{X_2}{S} = 15.4$. $\frac{X_3}{S} = 10$.

The time step is listed in the caption of each figure together with $h_{\min}$, the side length of the smallest finite element of the mesh (FVS rectangle). We have taken care to show the results of a large time step for Figures 4 and 6. If the time steps are increased by 20%, the computations blow up for these two cases. To have a rough idea of the CFL number in our finite element computations, keep in mind that the maximum velocities are 1 and $\frac{3}{2}$ for these two benchmark problems.

6 Discussion

In this paper, we have provided rigorous stability and error analysis of schemes that employ C^1 finite elements for velocity, and numerical tests, that lend credence to the notion that simple and efficient finite-element schemes based on the use of the well-posed pressure formula (1.4) may work well even if the standard inf-sup (LBB) stability condition does not hold.

As the inf-sup condition is most readily understood in the time-independent linear case, however, it seems worthwhile to briefly discuss that case in order to better understand how finite element methods based on UNSE may work regardless of whether the inf-sup condition holds or not.

6.1 Inf-sup condition for steady flow

Recall, for the mixed inhomogeneous Stokes problem

$$\nabla p - \Delta \boldsymbol{u} = \boldsymbol{f}, \quad \nabla \cdot \boldsymbol{u} = 0, \quad \boldsymbol{u}|_\Gamma = 0, \tag{6.1}$$

that standard mixed methods with finite-element approximation spaces X_h and Y_h for velocity and pressure take the form

$$\langle \nabla \boldsymbol{u}_h, \nabla \boldsymbol{v}_h \rangle - \langle p_h, \nabla \cdot \boldsymbol{v}_h \rangle = \langle \boldsymbol{f}, \boldsymbol{v}_h \rangle, \quad \forall \boldsymbol{v}_h \in X_h, \tag{6.2}$$

$$\langle \nabla \cdot \boldsymbol{u}_h, q_h \rangle = 0, \qquad\qquad\qquad \forall q \in Y_h. \tag{6.3}$$

A fundamental fact for this system is that the existence and boundedness of the solution map from $\boldsymbol{f} \in H^{-1}$ to $(\boldsymbol{u}_h, p_h)$ in $H_0^1 \times L^2$ is equivalent to the famous inf-sup condition: there should exist $c_h > 0$ such that

$$\inf_{q_h \in Y_h} \sup_{\boldsymbol{v}_h \in X_h} \frac{\langle \nabla \cdot \boldsymbol{v}_h, q_h \rangle}{\|\nabla \boldsymbol{v}_h\| \|q_h\|} \geq c_h > 0. \tag{6.4}$$

Also, the solution map is uniformly bounded in h if and only if c_h is uniformly bounded away from zero (see [9]). The main role of the inf-sup condition (6.4) lies in ensuring uniformly bounded solvability for the pressure from (6.2). If the condition fails to hold, methods typically encounter spurious pressure modes that destroy solvability or degrade accuracy.

6.2 Reformulation

Despite the well-known existence of a global Leray weak solution, well-posedness (existence and uniqueness) for the Navier-Stokes equations at present requires one to consider more regular

strong solutions locally in time, and this is the framework in which we proved local-time well-posedness for UNSE in [20]. By analogy, we introduce a corresponding strong reformulation of the Stokes problem above. Let $\lambda \geq 0$ and consider

$$\nabla p - \Delta \boldsymbol{u} = \boldsymbol{f}, \quad \boldsymbol{u}|_\Gamma = 0, \tag{6.5}$$

$$\langle \nabla p, \nabla q \rangle = \langle \boldsymbol{f} + \lambda \boldsymbol{u}, \nabla q \rangle + \langle \nabla \times \boldsymbol{u}, \boldsymbol{n} \times \nabla q \rangle_\Gamma, \quad \forall q \in H^1(\Omega). \tag{6.6}$$

We require $\boldsymbol{f} \in L^2(\Omega, \mathbb{R}^N)$ and seek $\boldsymbol{u} \in H^2 \cap H_0^1(\Omega, \mathbb{R}^N)$, $p \in H^1(\Omega)/\mathbb{R}$.

We claim that if Ω is bounded with C^3 boundary, this PDE problem is always well-posed and yields the solution of (6.1). A clean way to prove this is by operator theory. (We point out immediately that the usual inf-sup condition as in (6.4) will not be relevant for this formulation, because the pressure is stably determined by a Poisson equation, not from (6.2).) The pressure gradient in (6.6) is given by

$$\nabla p = (I - \mathcal{P})\boldsymbol{f} + B_\lambda \boldsymbol{u}, \quad \text{where } B_\lambda \boldsymbol{u} = \lambda(I - \mathcal{P})\boldsymbol{u} + \nabla p_{\mathrm{S}}(\boldsymbol{u}), \tag{6.7}$$

in terms of the Stokes pressure $\nabla p_{\mathrm{S}}(\boldsymbol{u})$. Thus (6.5) can be written as

$$A\boldsymbol{u} + B_\lambda \boldsymbol{u} = \mathcal{P}\boldsymbol{f}, \tag{6.8}$$

where the operator $A = -\Delta$, regarded as an unbounded operator on $L^2(\Omega, \mathbb{R}^N)$ with domain $D(A) = H^2 \cap H_0^1(\Omega, \mathbb{R}^N)$, is a positive self-adjoint operator with compact resolvent. It is a simple consequence of Theorem 1.1 and interpolation that there exist positive constants a and K with $a < 1$, such that for all $\boldsymbol{u} \in D(A)$,

$$\|B_\lambda \boldsymbol{u}\| \leq a\|A\boldsymbol{u}\| + K\|\boldsymbol{u}\|. \tag{6.9}$$

From a theorem on perturbation of sectorial operators (see [14, Theorem 1.3.2]), it is not difficult to show, by using expansions in eigenfunctions of A (details omitted), that $A + B_\lambda$ is sectorial with the same domain as A. Due to the identity

$$(\mu - A - B_\lambda)^{-1} = (\mu - A)^{-1} + (\mu - A)^{-1} B_\lambda (\mu - A - B_\lambda)^{-1},$$

the resolvent is compact, and it follows that the spectrum of $A + B_\lambda$ is discrete, consisting only of isolated eigenvalues of finite multiplicity.

It remains to show that zero is not an eigenvalue of $A + B_\lambda$. Suppose that $\boldsymbol{u} \in H^2 \cap H_0^1(\Omega, \mathbb{R}^N)$ satisfies $(A + B_\lambda)\boldsymbol{u} = 0$. This means

$$0 = -\Delta \boldsymbol{u} + (I - \mathcal{P})\Delta \boldsymbol{u} - \nabla \nabla \cdot \boldsymbol{u} + \lambda(I - \mathcal{P})\boldsymbol{u}, \tag{6.10}$$

hence dotting with ∇q where $q = -\nabla \cdot \boldsymbol{u}$, we find

$$0 = \|\nabla \nabla \cdot \boldsymbol{u}\|^2 + \lambda\|\nabla \cdot \boldsymbol{u}\|^2. \tag{6.11}$$

It follows $\nabla \cdot \boldsymbol{u} = 0$ (if $\lambda = 0$ the integral of the constant $\nabla \cdot \boldsymbol{u}$ is zero by boundary conditions) and therefore $\boldsymbol{u} = \mathcal{P}\boldsymbol{u}$. Hence $\boldsymbol{u} = 0$, since by (6.10) it now follows

$$0 = \langle -\mathcal{P}\Delta \boldsymbol{u}, \boldsymbol{u} \rangle = \langle -\Delta \boldsymbol{u}, \mathcal{P}\boldsymbol{u} \rangle = \|\nabla \boldsymbol{u}\|^2.$$

By consequence, zero lies in the resolvent set of $A + B_\lambda$, so that $(A + B_\lambda)^{-1}$ is bounded on $L^2(\Omega, \mathbb{R}^N)$ and equation (6.8) always has a solution bounded by the data (even if $\mathcal{P}\boldsymbol{f}$ is replaced by any $\boldsymbol{g} \in L^2(\Omega, \mathbb{R}^N)$). This solution, in fact, has zero divergence, which follows by dotting (6.8) with ∇q where $q = \nabla \cdot \boldsymbol{u}$. Again, we get (6.11), hence $\nabla \cdot \boldsymbol{u} = 0$.

6.3 A stable discretization

In discretizing the reformulation (6.5)–(6.6), of course $\boldsymbol{u}$ and p are coupled together; there is no simple decoupling analogous to splitting time steps in the time-dependent case. It is nevertheless relevant to note that if the velocity is known, pressure will be determined by solving a discrete Poisson equation. For this reason, we can expect that the inf-sup condition (6.4) will have no role in determining the stability or accuracy of pressure in this approach, and we can expect no spurious pressure modes.

Instead the issue becomes whether the velocity can be stably determined by approximation schemes without regard to (6.4). A typical finite-element discretization will provide an approximation to the operator $A + B_\lambda$ in (6.8) acting in a finite-element space $X_{0,h}$ for velocity. The issue is whether this non-selfadjoint discrete operator has a uniformly bounded inverse.

This question does not seem easy to resolve in general, but we will illustrate by proving stability for a finite-element scheme from [23] for (6.5)–(6.6), that uses C^1 elements for velocity and C^0 elements for pressure with no need for the inf-sup condition (6.4). (The method is not practical, but that is not the point.) The idea behind the scheme comes from the identity

$$\langle -\Delta\boldsymbol{u} + \lambda(I - \mathcal{P})\boldsymbol{u}, -\Delta\boldsymbol{u} + \lambda\mathcal{P}\boldsymbol{u}\rangle = \|\Delta\boldsymbol{u}\|^2 + \lambda\|\nabla\boldsymbol{u}\|^2, \tag{6.12}$$

together with the estimate coming from Theorem 1.1,

$$|\langle \nabla p_{\mathrm{s}}(\boldsymbol{u}), \Delta\boldsymbol{u}\rangle| \leq \frac{1}{2}\|\nabla p_{\mathrm{s}}\|^2 + \frac{1}{2}\|\Delta\boldsymbol{u}\|^2 \leq a\|\Delta\boldsymbol{u}\|^2 + C_a\|\nabla\boldsymbol{u}\|^2 \tag{6.13}$$

for $a \in (0, 1)$ independent of $\boldsymbol{u}$. If $\lambda > C_a$, then for any nonzero $\boldsymbol{u} \in H^2 \cap H_0^1(\Omega, \mathbb{R}^N)$,

$$\langle -\Delta\boldsymbol{u} + B_\lambda\boldsymbol{u}, -\Delta\boldsymbol{u} + \lambda\mathcal{P}\boldsymbol{u}\rangle \geq (1 - a)\|\Delta\boldsymbol{u}\|^2 + (\lambda - C_a)\|\nabla\boldsymbol{u}\|^2. \tag{6.14}$$

Thus the bilinear form on the left-hand side is coercive in $H^2 \cap H_0^1(\Omega, \mathbb{R}^N)$, meaning that the bounded solvability of (6.5)–(6.6) can be ensured by applying the Lax-Milgram theorem to the weak-form problem of finding $\boldsymbol{u} \in X = H^2 \cap H_0^1(\Omega, \mathbb{R}^N)$ such that

$$\langle -\Delta\boldsymbol{u} + B_\lambda\boldsymbol{u}, -\Delta\boldsymbol{v} + \lambda\mathcal{P}\boldsymbol{v}\rangle = \langle \mathcal{P}\boldsymbol{f}, -\Delta\boldsymbol{v} + \lambda\mathcal{P}\boldsymbol{v}\rangle, \quad \forall \boldsymbol{v} \in X. \tag{6.15}$$

A corresponding stable finite-element scheme can be obtained as follows. Let $X_{0,h} \subset H^2 \cap H_0^1(\Omega, \mathbb{R}^N)$ and $Y_h \subset H^1(\Omega)/\mathbb{R}$ be spaces for approximate velocity and pressure as before. A discrete Leray projection $\mathcal{P}_h$ is defined as follows: For any $\boldsymbol{a} \in L^2(\Omega, \mathbb{R}^N)$, define $\phi_h \in Y_h$ by solving

$$\langle \nabla\phi_h, \nabla q_h\rangle = \langle \boldsymbol{a}, \nabla q_h\rangle, \quad \forall q_h \in Y_h. \tag{6.16}$$

Then $\mathcal{P}_h\boldsymbol{a} := \boldsymbol{a} - \nabla\phi_h$. Note $\langle \mathcal{P}_h\boldsymbol{a}, (I - \mathcal{P}_h)\boldsymbol{b}\rangle = 0$ for any $\boldsymbol{a}, \boldsymbol{b} \in L^2(\Omega, \mathbb{R}^N)$, and $\|I - \mathcal{P}_h\| = 1$. By dotting (6.5) by the test function $-\Delta\boldsymbol{v} + \lambda\mathcal{P}\boldsymbol{v}$ and discretizing (for convenience letting p_h

denote an approximation to $p - \mathcal{Q}\boldsymbol{f}$ where $\nabla \mathcal{Q}\boldsymbol{f} = (I - \mathcal{P})\boldsymbol{f}$), we obtain the following C^1 finite element scheme for steady-state Stokes equations: Find $\boldsymbol{u}_h \in X_{0,h}$ and $p_h \in Y_h$ so that

$$\langle -\Delta \boldsymbol{u}_h + \nabla p_h, -\Delta \boldsymbol{v}_h + \lambda \mathcal{P}_h \boldsymbol{v}_h \rangle = \langle \mathcal{P}_h \boldsymbol{f}, -\Delta \boldsymbol{v}_h + \lambda \mathcal{P}_h \boldsymbol{v}_h \rangle, \tag{6.17}$$

$$\langle \nabla p_h - \lambda \boldsymbol{u}_h - \Delta \boldsymbol{u}_h + \nabla \nabla \cdot \boldsymbol{u}_h, \nabla q_h \rangle = 0 \tag{6.18}$$

for all $\boldsymbol{v}_h \in X_{0,h}$ and $q_h \in Y_h$.

For large $\lambda > 0$ this scheme has a solution uniformly bounded in terms of the data, for arbitrary spaces $X_{0,h}$ and Y_h regardless of (6.4). For the proof, note (6.18) yields

$$\nabla p_h = \lambda(I - \mathcal{P}_h)\boldsymbol{u}_h + (I - \mathcal{P}_h)\nabla p_{\mathrm{s}}(\boldsymbol{u}_h), \tag{6.19}$$

since the Stokes pressure satisfies (1.8). Plug this into the left-hand side of (6.17). The resulting bilinear form on the left-hand side of (6.17) is coercive, since choosing $\boldsymbol{v}_h = \boldsymbol{u}_h$ and arguing as in (6.12)–(6.14) above yields

$$\langle -\Delta \boldsymbol{u}_h + \lambda(I - \mathcal{P}_h)\boldsymbol{u}_h, -\Delta \boldsymbol{u}_h + \lambda \mathcal{P}_h \boldsymbol{u}_h \rangle - \langle (I - \mathcal{P}_h)\nabla p_{\mathrm{s}}(\boldsymbol{u}_h), \Delta \boldsymbol{u}_h \rangle$$
$$\geq (1 - a)\|\Delta \boldsymbol{u}_h\|^2 + (\lambda - C_a)\|\nabla \boldsymbol{u}_h\|^2. \tag{6.20}$$

A standard use of the Lax-Milgram theorem finishes the proof.

For further details, error estimates and related results, see the Ph. D. thesis of the second author [23].

References

[1] Armaly, B. F., Durst, F., Pereira, J. C. F., et al, Experimental and theoretical investigation of backward-facing step flow, *J. Fluid Mech.*, **127**, 1983, 473–496.

[2] Barth, T., Bochev, P., Gunzburger, M., et al, A taxonomy of consistently stabilized finite element methods for the Stokes problem, *SIAM J. Sci. Comput.*, **25**, 2004, 1585–1607.

[3] Bochev, P. B., Dohrmann, C. R., and Gunzburger, M. D., Stabilization of low-order mixed finite elements for the Stokes equations, *SIAM J. Numer. Anal.*, **44**, 2006, 82–101.

[4] Brown, D. L., Cortez, R. and Minion, M. L., Accurate projection methods for the incompressible Navier-Stokes equations, *J. Comput. Phys.*, **168**, 2001, 464–499.

[5] Botella, O. and Peyret, R., Benchmark spectral results on the lid-driven cavity flow, *Comput. Fluids*, **27**, 1998, 421–433.

[6] Ciarlet, P. G., The Finite Element Methods for Elliptic Problems, North Holland, Amsterdam, 1978.

[7] E, W. and Liu, J.-G., Gauge method for viscous incompressible flows, *Commun. Math. Sci.*, **1**, 2003, 317–332.

[8] de Veubeke, B. F., A conforming finite element for plate bending, *Int. J. Solids Structures*, **4**, 1968, 95–108.

[9] Girault, V. and Raviart, P-A., Finite Element Methods for Navier-Stokes Equations: Theory and Algorithms, Springer-Verlag, Berlin, 1986.

[10] Grubb, G. and Solonnikov, V. A., Reduction of the basic initial-boundary value problems for the Navier-Stokes equations to initial-boundary value problems for nonlinear parabolic systems of pseudodifferential equations, *J. Soviet Math.*, **56**, 1991, 2300–2308.

[11] Grubb, G. and Solonnikov, V. A., Boundary value problems for the nonstationary Navier-Stokes equations treated by pseudodifferential methods, *Math. Scand.*, **69**, 1991, 217–290.

[12] Guermond, J. L., Minev, P. and Shen, J., An overview of projection methods for incompressible flows, *Comput. Methods Appl. Mech. Eng.*, **195**(44–47), 2006, 6011–6045.

[13] Guermond, J. L. and Shen, J., A new class of truly consistent splitting schemes for incompressible flows, *J. Comput. Phys.*, **192**, 2003, 262–276.

[14] Henry, D., Geometric Theory of Semilinear Parabolic Equations, Lecture Notes in Mathematics, **840**, Springer-Verlag, Berlin, 1981.

[15] Henshaw, W. D. and Petersson, N. A., A split-step scheme for the incompressible Navier-Stokes equations, Numerical Simulations of Incompressible Flows, World Scientific, River Edge, 2003, 108–125.

[16] Johnston, H. and Liu, J.-G., Accurate, stable and efficient Navier-Stokes solvers based on explicit treatment of the pressure term, *J. Comput. Phys.*, **199**(1), 2004, 221–259.

[17] Karniadakis, G. E., Israeli, M. and Orszag, S. A., High-order splitting methods for the incompressible Navier-Stokes equations, *J. Comput. Phys.*, **97**, 1991, 414–443.

[18] Kim, J. and Moin, P., Application of a fractional-step method to incompressible Navier-Stokes equations, *J. Comput. Phys.*, **59**, 1985, 308–323.

[19] Lai, M. J. and Schumaker, L. L., On the approximation power of splines on triangulated quadrangulations, *SIAM J. Numer. Anal.*, **36**, 1999, 143–159.

[20] Liu, J.-G., Liu, J. and Pego, R. L., Stability and convergence of efficient Navier-Stokes solvers via a commutator estimate, *Comm. Pure Appl. Math.*, **60**, 2007, 1443–1487.

[21] Liu, J.-G. and Pego, R. L., Stable discretization of magnetohydrodynamics in bounded domains, *Comm. Math. Sci.*, 2009, to appear.

[22] Leriche, E., Perchat, E., Labrosse, G., et al, Numerical evaluation of the accuracy and stablity properties of high-order direct Stokes solvers with or without temporal splitting, *J. Sci. Comput.*, **26**, 2006, 25–43.

[23] Liu, J., A class of efficient, stable Navier-Stokes solvers, Ph. D. thesis, University of Maryland, 2006.

[24] Orszag, S. A., Israeli, M. and Deville, M., Boundary conditions for incompressible flows, *J. Sci. Comput.*, **1**, 1986, 75–111.

[25] Sani, R. L., Shen, J., Pironneau, O., et al, Pressure boundary condition for the time-dependent incompressible Navier-Stokes equations, *Int. J. Numer. Meth. Fluids*, **50**, 2006, 673–682.

[26] Soane, A. M. and Rostamian, R., Variational problems in weighted Sobolev spaces on non-smooth domains, preprint.

[27] Timmermans, L. J. P., Minev, P. D. and van de Vosse, F. N., An approximate projection scheme for incompressible flow using spectral elements, *Int. J. Numer. Meth. Fluids*, **22**, 1996, 673–688.